Influence of the amount of intermetallics on the degradation of Mg-Nd alloys under physiological conditions

Zhang, Yaping; Huang, Yuanding; Feyerabend, Frank; Blawert, Carsten; Gan, Weimin; Maawad, Emad; You, Sihang; Gavras, Sarkis; Scharnagl, Nico; Bode, Julia; Vogt, Carla; Zander, Daniela; Willumeit-Römer, Regine; Kainer, Karl Ulrich; Hort, Norbert

Published in:
Acta Biomaterialia

DOI:
10.1016/j.actbio.2020.11.050

Publication date:
2021

Document Version
Publisher's PDF, also known as Version of record

Acta Biomaterialia 121 (2021) 695–712

Contents lists available at ScienceDirect

Acta Biomaterialia

journal homepage: www.elsevier.com/locate/actbio

Influence of the amount of intermetallics on the degradation of Mg-Nd alloys under physiological conditions

Yaping Zhang[a,*], Yuanding Huang[a], Frank Feyerabend[a], Carsten Blawert[a], Weimin Gan[b], Emad Maawad[a], Sihang You[a], Sarkis Gavras[a], Nico Scharnagl[a], Julia Bode[c], Carla Vogt[c], Daniela Zander[d], Regine Willumeit-Römer[a], Karl Ulrich Kainer[a,e], Norbert Hort[a]

[a] Institute of Materials Research, Helmholtz-Zentrum Geesthacht, Max-Planck-Straβe 1, 21502 Geesthacht, Germany
[b] GEMS at MLZ, Helmholtz-Zentrum Geesthacht, Lichtenberg Straβe 1, 85747 Garching, Germany
[c] Institut für Analytische Chemie, TU Bergakademie Freiberg, Leipziger Straβe 29, 09599 Freiberg, Germany
[d] Division of Materials Science and Engineering, RWTH Aachen University, Intzestraβe 5, 52072 Aachen, Germany
[e] Chair of Light Elements Engineering, Foundry and Automation, Wrocław University of Science and Technology, 50-370 Wrocław, W. Wyspianskiego 27, Poland

ARTICLE INFO

Article history:
Received 25 September 2020
Revised 4 November 2020
Accepted 29 November 2020
Available online 3 December 2020

Keywords:
Magnesium-neodymium alloys
Intermetallic particles
Degradation
Microstructure

ABSTRACT

The influence of amount of intermetallics on the degradation of as-extruded Mg-Nd alloys with different contents of Nd was investigated via immersion testing in DMEM+10% FBS under cell culture conditions and subsequent microstructural characterizations. It is found that the presence of intermetallic particles $Mg_{41}Nd_5$ affects the corrosion of Mg-Nd alloys in two conflicting ways. One is their negative role that their existence enhances the micro-galvanic corrosion. Another is their positive role. Their existence favours the formation of a continuous and compact corrosion layer. At the early stage of immersion, their negative role predominated. The degradation rate of Mg-Nd alloys monotonously increases with increasing the amount of intermetallics. Mg-5Nd alloy with maximum amount of intermetallics suffered from the most severe corrosion. With the immersion proceeding (≥7 days), then the positive role of these intermetallic particles $Mg_{41}Nd_5$ could not be neglected. Owing to the interaction between their positive and negative roles, at the later stage of immersion the corrosion rate of Mg-Nd alloys first increases with increasing the content of Nd, then reaches to the maximum at 2 wt. % Nd. With a further increase of Nd content, a decrease in corrosion rate occurs. The main corrosion products on the surfaces of Mg-Nd alloys include carbonates, calcium-phosphate, neodymium oxide and/or neodymium hydroxide. They are amorphous at the early stage of immersion. With the immersion proceeding, they are transformed to crystalline. The existence of undegradable $Mg_{41}Nd_5$ particles in the corrosion layer can enhance the crystallization of such amorphous corrosion products.

Statement of significance

Many of the current developed biodegradable magnesium alloys contain intermetallics due to the requirements by improving their strength. The existence of intermetallics is normally considered to have a negative effect on the corrosion resistance of magnesium alloys owing to the occurrence of micro-galvanic corrosion. Understanding how to balance the corrosion resistance and mechanical properties through the control of intermetallic microstructure plays a key role in developing new biodegradable magnesium alloys with high performance. Therefore, the present work selected Mg-Nd alloys to investigate the influence of intermetallic amount and distribution on their corrosion properties. The "coin effect" of intermetallics on corrosion resistance was concluded: one well-known negative role enhancing the corrosion and another positive role alleviating the corrosion.

* Corresponding author.
E-mail address: yaping.zhang@hzg.de (Y. Zhang).

https://doi.org/10.1016/j.actbio.2020.11.050
1742-7061/

1. Introduction

Numerous recent studies have emphasized that magnesium and its alloys could work as temporary implants due to their good biocompatibility, density (1.74-2.0 g/cm^3), compressive yield stress (65-100 MPa) and elastic modulus (41- 45 GPa), which are fairly close to that of natural bones [1–3]. The main obstacle for their applications is to balance the strength and degradation rate. The improvement of strength of magnesium alloys can be achieved through grain refinement, solid solution and precipitation strengthening [4–6]. Among them, precipitation strengthening is one of the most popular approach [7]. Many of the already developed biodegradable magnesium alloys contain intermetallics [8–11]. The intermetallic phases can act as either a continuous network barrier to retard corrosion propagation [12], or as a galvanic cathode to accelerate corrosion of the Mg matrix [9], or as a micro-anode to dissolve preferentially at the initial corrosion stage [10].

The intermetallics inside the alloys greatly influence the corrosion resistance related to their microstructure (amount, distribution and electrochemical property (cathodic or anodic) etc.) [11,13,14]. For example, in as-cast Mg-Al alloy, if the cathodic $Mg_{17}Al_{12}$ phase possesses a small fraction, an increase of $Mg_{17}Al_{12}$ phase will lead to a higher corrosion rate due to the micro-galvanic corrosion in NaCl solution. If there is a high percentage of $Mg_{17}Al_{12}$ phase with a net-like distribution along the grain boundaries, it will act mainly as a barrier against the corrosion of the matrix [15,16]. Similar features were found for both as-cast and extruded Mg-xZn alloys (x $\leq$ 5 wt. %) immersed in the NaCl solution [17,18]. When the volume fraction of cathodic MgZn phase is low, an increase in its amount has a detrimental effect on the corrosion resistance because of an increase in the galvanic effect between the matrix and MgZn phase. Contrary to this, in simulated body fluid (SBF), an increase of small amount of intermetallics has a positive effect on the corrosion resistance of as-cast Mg-xZn alloys (x $\leq$ 5 wt. %) due to the formation of a protective Zn-containing film. However, a high volume fraction of continuous MgZn phase accelerates the corrosion rate of as-cast Mg-7Zn alloy due to the presence of more anode-cathode sites [19]. While in as-cast and as-extruded Mg-xCa alloys (x $\leq$ 3 wt. %), their corrosion resistance decreases with increasing volume fraction of both continuous and discontinuous anodic Mg_2Ca phase in Hank's solution [20].

Besides the above-mentioned RE (Rare earth)-free alloys, the intermetallic amount also affects the corrosion properties of RE-containing magnesium alloys. In the as-cast Mg-La, Mg-Ce, Mg-Nd and Mg-Y alloys, an increase of intermetallics leads to an increase of their corrosion rate in NaCl solution [21–23]. However, different results were also reported for as-cast Mg-xNd alloys (x = 1, 4 wt. %). In these alloys [24] their corrosion rate changed inversely. It decreased with an increasing amount of $Mg_{12}Nd$ phase when immersed in NaCl solution. The assumption was that Nd ions were incorporated into the surface hydroxide layer which protected the matrix from the aggression of Cl^-. Regarding this Mg-Nd binary system, when further increasing the content of Nd to more than 4.0 wt. % the corrosion rate increased again with increasing the volume fraction of $Mg_{12}Nd$ phase. The influence of intermetallic amount on the corrosion also depends on the corrosion environment. The uses of different corrosion media could change the corrosion behaviours for the same alloy. For example, in the swage forged Mg-Y alloys with increasing the intermetallic amount, their corrosion rates increased in NaCl solution but decreased in Na_2SO_4 solution. The different evolutions of corrosion rates are attributed to the enhanced formation of Y-containing protective surface film when these alloys were immersed in the Na_2SO_4 solution [25].

Although the influence of intermetallic amount on the corrosion was investigated, it was normally performed using as-cast samples. Regarding these as-cast alloys which contain high contents of alloying elements, large amount of intermetallics could be formed at the dendritic and grain boundaries. They are distributed continuously at these places. Previous investigations indicated that such a continuous distribution at boundaries possibly creates barriers to the propagation of corrosion, and consequently improve the corrosion resistance. That is to say, the intermetallic amount could affect its distribution, and then further influence corrosion resistance. In addition, the effects of intermetallic amount on the corrosion behaviour was previously investigated using simple electrolytes such as NaCl solution, which is far away from our body fluid. Moreover, as aforementioned, when investigating the influence of intermetallic amount on the corrosion of magnesium alloys different results were obtained by different investigators, even some of them were controversial. In order to further clarify these points and to avoid the disturbance caused by the intermetallic distribution, in the present investigation as-extruded Mg-xNd alloys were selected. The applied corrosion agent is much more complicated using DMEM (Dulbecco's modified eagle's medium) with 10% FBS (Fetal bovine serum) under cell culture conditions. The influence of Nd-containing intermetallic amount on the corrosion of Mg-Nd alloys was systematically explored using the immersion test, SKPFM (Scanning kelvin probe force microscopy), ToF-SIMS (Time of flight secondary ion mass spectroscopy) and synchrotron radiation. The related mechanisms are discussed.

2. Experimental

In order to investigate the influence of amount of intermetallics on the degradation of as-extruded Mg-Nd alloys with different contents of Nd in DMEM+10% FBS under cell culture conditions, the following experiments were performed. A detailed procedure was schematically shown in Fig. 1.

2.1. Materials

Mg-xNd alloys (x = 0, 0.5, 2, 5 wt. %) were prepared using permanent mould direct chill casting [26]. Pure Mg (Magnesium Electron, Manchester, UK, 99.94 wt. %) was first melted in a mild steel crucible (1.0044, EU Grade) with an atmospheric protection cover gas of Ar + 2% SF_6. Then pure Nd (Grirem, Beijing, China, 99.5 wt. %) was added to the melt at a temperature of 750°C. After being stirred at 200 rpm for 20 minutes, the melt was then poured into a preheated mild steel mould (500°C) covered with a mould release agent (boron nitride). The diameter of the mould was 100 mm and its length was 220 mm. The filled mould was held at 670°C for 30 minutes under protective atmosphere (Ar + 2% SF_6), then lowered into circulating cooling water at a rate of 10 mm/s for solidification. When it was fully immersed, the mould was held in cooling water for 10 seconds and then removed from the water tank.

The as-cast ingots were machined to extrusion billets with a diameter of 93 mm and a length of 200 mm. After being homogenized in an electromagnetic induction furnace at 440°C for 30 minutes, they were indirectly extruded to cylindrical bars with a diameter of 12 mm at 450°C, followed by air-cooling. The extrusion ratio was 1: 63 and the ram speed was 0.6 mm/s. After extrusion, one sample from the middle of extruded bar was used for chemical analysis using spark discharge optical emission spectroscopy (SD – OES, Spectrolab, M. Spectro Analytical Instrument GmbH, Kleve, Germany) with "Spark Analyse Vision" software.

2.2. Microstructural observations

At least four samples were duplicated for microstructural observations for each alloy. Three of them were prepared by grinding, mechanical polishing and etching according to that reported

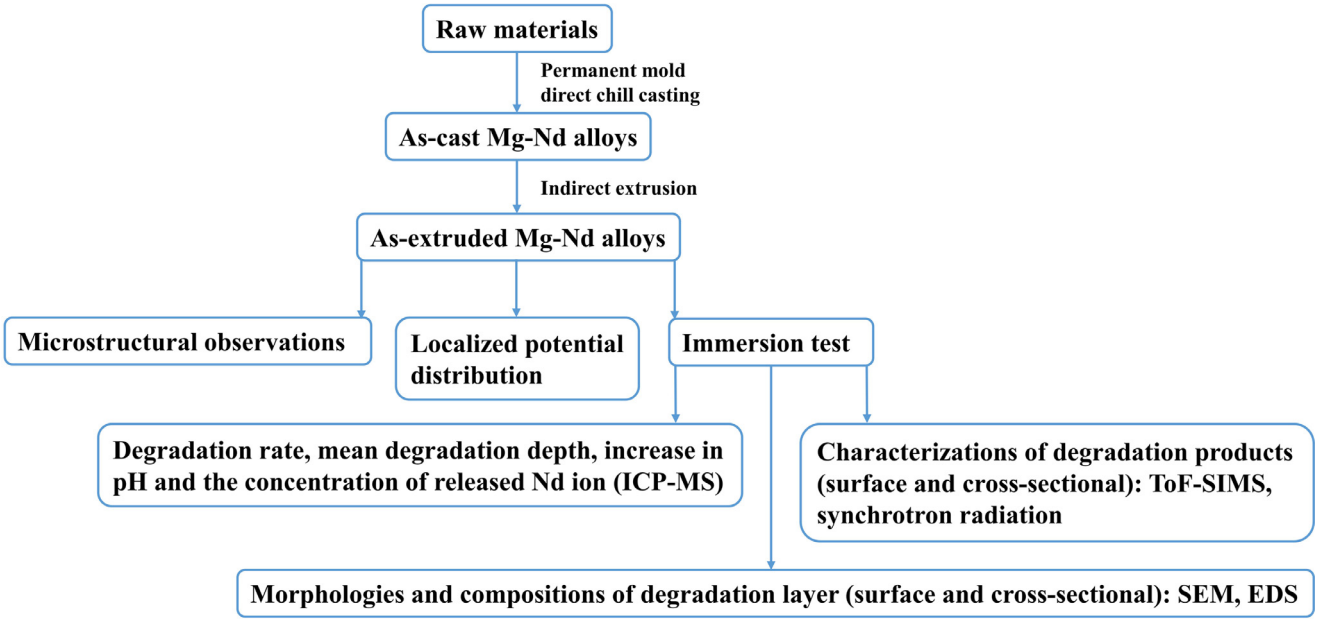

Fig. 1. Schematic illustration of the experimental procedure performed in this work.

by Kree *et al.* [27] and Hort *et al.* [28]. The etchant was a mixture of 8 g picric acid (Sigma-Aldrich Chemie GmbH, Munich, Germany), 5 mL acetic acid (Avantor Performance Materials B.V., Arnhem, Netherlands), 10 mL distilled water and 100 mL ethanol (REHER & RAMSDEN NACHFLG. GmbH & Co. KG, Hamburg, Germany). Microstructures were characterized by an optical microscope (LEICA DMLM, Leica Microsystems Wetzlar GmbH, Wetzlar, Germany) equipped with a digital camera and a scanning electron microscope (SEM, Tescan Vega3 SB, Brno, Czech Republic) equipped with an energy dispersive X-ray analyser (EDS, Eumex Instrumentebau GmbH, Heidenrod, Germany). Grain size analysis was performed using the linear intercept method according to ASTM E 112-13 [29]. The volume fraction of intermetallics was statistically measured using backscattered electron (BSE) micrographs captured from different regions and calculated by ImageJ software (National Institutes of Health, Version 1.51k). Thermodynamic predictions were performed using Pandat software (Compu Therm LLC, Version 2017) with the database PanMg2017. During thermodynamic prediction, the non-equilibrium Scheil solidification model was used to calculate the volume fraction of the intermetallic phase in Mg-Nd alloys. The detailed descriptions about the non-equilibrium Scheil solidification model can be found elsewhere [30]. The remaining sample was used for transmission electron microscopy (TEM) observations with a CM200 (Philips & Co., Eindhoven, Netherland) operating at 200 kV. TEM foils were prepared by electropolishing in a twin jet system using a solution of 1.5% $HClO_4$ and 98.5% ethanol at -50°C and a voltage of 50 V.

2.3. Localized potential distribution

Scanning kelvin probe force microscopy (SKPFM) based on an atomic force microscopy (AFM, NanoWizard® AFM, JPK Instruments AG, Berlin, Germany) was used to measure the relative Volta potential difference between the intermetallic phase and Mg matrix in alternating current (AC) mode. A silicon probe (Budgetsensors, Multi75E-G, Innovative Solutions Bulgaria Ltd., Sofia, Bulgaria) coated with Pt-Cr layer was used for SKPFM tests. The resonance frequency and force constant of the silicon probe were 75 kHz and 3 N/m, respectively. The distance between the sample surface and probe was set at 100 nm. Data were analysed by JPK Data Processing software (JPK Instruments AG, Version spm-6.1.49). Prior to SKPFM tests, one sample was prepared by grinding and polishing according to the same method used for microstructural analysis. After polishing it was then immediately stored in a vacuum desiccator to avoid oxidation. SKPFM tests were conducted in ambient condition.

2.4. Immersion test

The schematic outline of similar immersion test procedure employed in the present work could be found in Ref. [31]. Discs with a dimension of 10 × 1.5 mm (diameter × height) were machined from the extruded bars for immersion tests. After ultrasonically cleaned by n-Hexane, acetone and 100% ethanol in sequence (each for 20 minutes), they were sterilized in 70% ethanol and dried on a clean bench (Heraeus BBD 6620, Thermo Fisher Scientific, Schwerte, Germany) under sterile conditions. The selected immersion medium is DMEM + Glutamax (Dulbecco's modified eagle's medium, (+) 4.5 g/L D-Glucose, (+) Pyruvate, Life Technologies, Darmstadt, Germany) together with 10% FBS (Fetal Bovine Serum, PAA Laboratories, Linz, Austria) in an incubator (Heraeus BBD 6620, Thermo Fisher Scientific, Schwerte, Germany) under cell culture conditions (37°C, 20% O_2, 5% CO_2 and 95% relative humidity). The details of this medium compositions were given by Fischer *et al.* [32].

Prior to immersion, the initial weight of samples was recorded. At least six samples were averaged for each alloy. According to the standard ISO 10993- 12 (2008), each sample was immersed in the medium at a ratio of 10 mL/g (medium: sample) [33]. During immersion, the immersion medium was changed every 2-3 days to keep semi-static immersion test conditions. The pH value (measured using a SENTRON ARGUS X pH-meter, Fisher Scientific GMBH, Schwerte, Germany) and the released Nd ion concentration (using ICP-MS, Inductively coupled plasma quadrupole mass spectrometry, iCAP Q, Thermo Fisher Scientific Inc., Waltham, USA) of immersion medium were measured before each medium change. The medium without samples was served as a control. After immersion, the corroded samples were cleaned with distilled water and 100% ethanol. Regarding the degradation rate analysis, a minimum of four specimens per incubation time was statistically

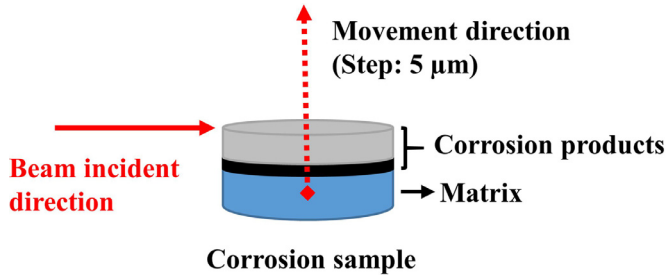

Fig. 2. Schematic illustration of phase identification by high-energy X-ray beamline HEMS P07B at PETRA III, DESY.

considered. The remaining two samples were kept to analyse the compounds and chemical compositions of the corrosion products on their surfaces. The degradation products were removed by immersion in chromic acid (180 g/L chromium (VI) oxide in distilled water, VWR international, Darmstadt, Germany) for 20 minutes at room temperature. After the removal of corrosion products, the samples were cleaned by vigorous shaking in distilled water and 100% ethanol. The additional immersions of initial samples (without corrosion) in chromic acid for 20 minutes indicated that their weights remained the same before and after immersion, confirming that the process of corrosion product removal using chromic acid could not bring any damage to the alloys. The degradation rate (DR) was then calculated according to the standard ASTM G31-72. In addition, the mean degradation depth (h) of corroded samples in µm was calculated using the following Eq. (1), which rationale was discussed by Nidadavolu *et al.* [31,34]:

$$h = \frac{10000 \times \Delta m}{A \times \rho} = \frac{DR \times t}{8.76} \quad (1)$$

where Δm is the weight loss in grams, A is the surface area of samples immersed in medium in cm^2, t is the immersion time in hours, ρ is the density of samples in g/cm^3 and DR is the degradation rate in mm/y. The actual densities of as-extruded pure Mg and Mg-Nd alloys were measured according to Archimedes' principle using 100% ethanol as a fluid and a balance (Sartorius LA 230S analytical balance, Sartorius Corporate Administration GmbH, Göttingen, Germany) for weighting.

2.5. Characterizations of degradation products

EDS mapping analysis was conducted to analyse the distributions of related elements in the corrosion layer of specimens. The samples immersed for 14 days were selected for evaluations. They were mounted in resin with their cross section oriented upwards, and then ground and polished. The element mapping was performed with a resolution of 256 pixels and an acquisition time of 80 ms per pixel. The data analysis was completed using Iridium Ultra software (IXRF System, Inc., Version 2.4F).

In order to identify the corrosion components, the synchrotron X-ray diffraction experiments were conducted at the side station of the High Energy Materials Science beamline (HEMS) of Helmholtz-Zentrum Geesthacht at PETRA III storage ring in DESY (Deutsches Elektronen Synchrotron, Hamburg, Germany). The wavelength and beam size were 0.014235 nm and 5 µm × 10 µm (width × length), respectively. Fig. 2 shows the schematic diagram of the experimental process.

Firstly, the position of corrosion sample was adjusted so that its corrosion surface aligned with the beam. Then, the sample was moved upwards with a step size of 5 µm. At each step, the radiation diffraction was performed and Debye-Scherrer rings were recorded using a Perkin Elmer XRD 1622 (PerkinElmer, Inc., Santa Clara, USA) detector with a distance of 1115 mm to the sample centre. The integrated intensities of images were calculated using FIT2D software (Hammersley, V12.077).

Table 1
Actual chemical compositions of alloys (wt. %).

Alloys	Nd	Fe	Cu	Ni	Mg
Pure Mg	-	0.0015	<0.0001	<0.0002	Balance
Mg-0.5Nd	0.68	0.0082	0.0019	0.0003	Balance
Mg-2Nd	2.39	0.0026	0.0021	0.0011	Balance
Mg-5Nd	>4.20	0.0160	0.0024	0.0038	Balance

The chemical composition of interfacial regions between the corrosion layer and matrix was analysed using ToF-SIMS (Time of flight secondary ion mass spectroscopy). It was carried out on an orthogonal extraction time-of-flight instrument (C-ToF, TOFWERK AG, Thun, Switzerland) equipped with a Cobra-FIB LMIS (Liquid metal ion source, TESCAN GmbH, Dortmund, Germany). The chamber was maintained at a pressure of 2.5×10^{-6} mbar. A highly focused primary $^{69}Ga^+$ ion beam was accelerated at 5 keV with a target current of 3.67 nA to scan across the corrosion layer and matrix (Fig. 3). The ToF-SIMS analysis was performed as follows: firstly, a drop of carbon glue (Ted Pella. Inc., Redding, USA) was placed at the edge of sample surface. After its drying, the sample was then polished with 1 μm diamond suspension (Schmitz Metallographie GmbH, Herzogenrath, Germany) and cleaned with 100% ethanol (Reher & Ramsden Nachflg. GmbH & Co. KG, Hamburg, Germany). Due to the difference in height and hardness between the carbon glue and corrosion product layer, a slope surface was then prepared after polishing, which resulted in the exposure of the inner corrosion layer. The resultant gradient surface was then tilted to be vertical to the primary $^{69}Ga^+$ ion beam. Finally, the primary ion beam was focused on the specified areas nearby the interface between the matrix and inner corrosion layer (indicated by the red double arrows).

2.6. Statistical analysis

All the data displayed as the arithmetical mean ± standard deviation (SD) were obtained from at least three independent and replicate experiments. Statistical analysis for degradation rates was performed using the software Origin 2019 (OriginLab Corporation, Northampton, USA). One-way analysis of variance (ANOVA) on ranks with Dunn's multiple comparison post hoc tests was applied.

3. Results

3.1. Chemical compositions

Table 1 lists the actual chemical compositions of investigated alloys. As the upper limit of Nd detection using Spark analyser is 4.2 wt. %, it is difficult to determine the Nd content for the as-extruded Mg-5Nd alloy accurately. Compared with the nominal compositions, all alloys show a slightly higher Nd-content than the nominal one. A little high amount of Fe was detected in Mg-5Nd alloy. It most likely derived from the raw materials or the tools used for melting and casting such as the steel mould and stirring tool.

3.2. Microstructural characterizations

The matrix compositions and microstructures of as-extruded Mg-Nd alloys are shown in Table 2 and Fig. 4(a-d), respectively. The matrix of as-extruded Mg-0.5Nd (indicated by M1 in Fig. 4(b)) contains less Nd than the as-extruded Mg-2Nd (indicated by M2 in Fig. 4(c)). When the addition amount of Nd is more than 2 wt. % in Mg, the Nd content in the matrix remains stable with a value of

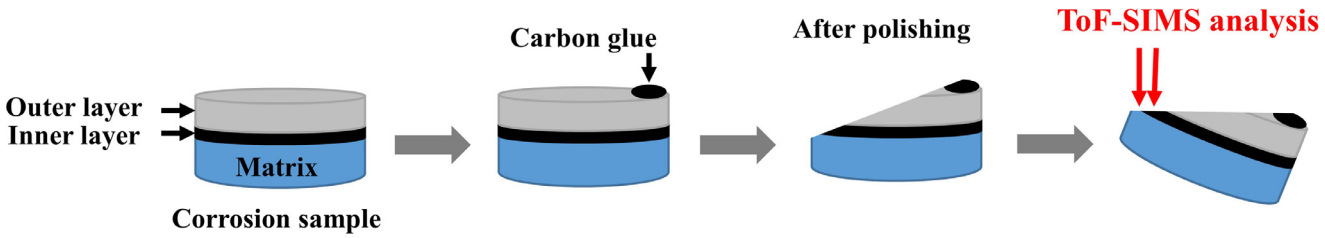

Fig. 3. Schematic diagrams of sample preparation for ToF-SIMS analysis.

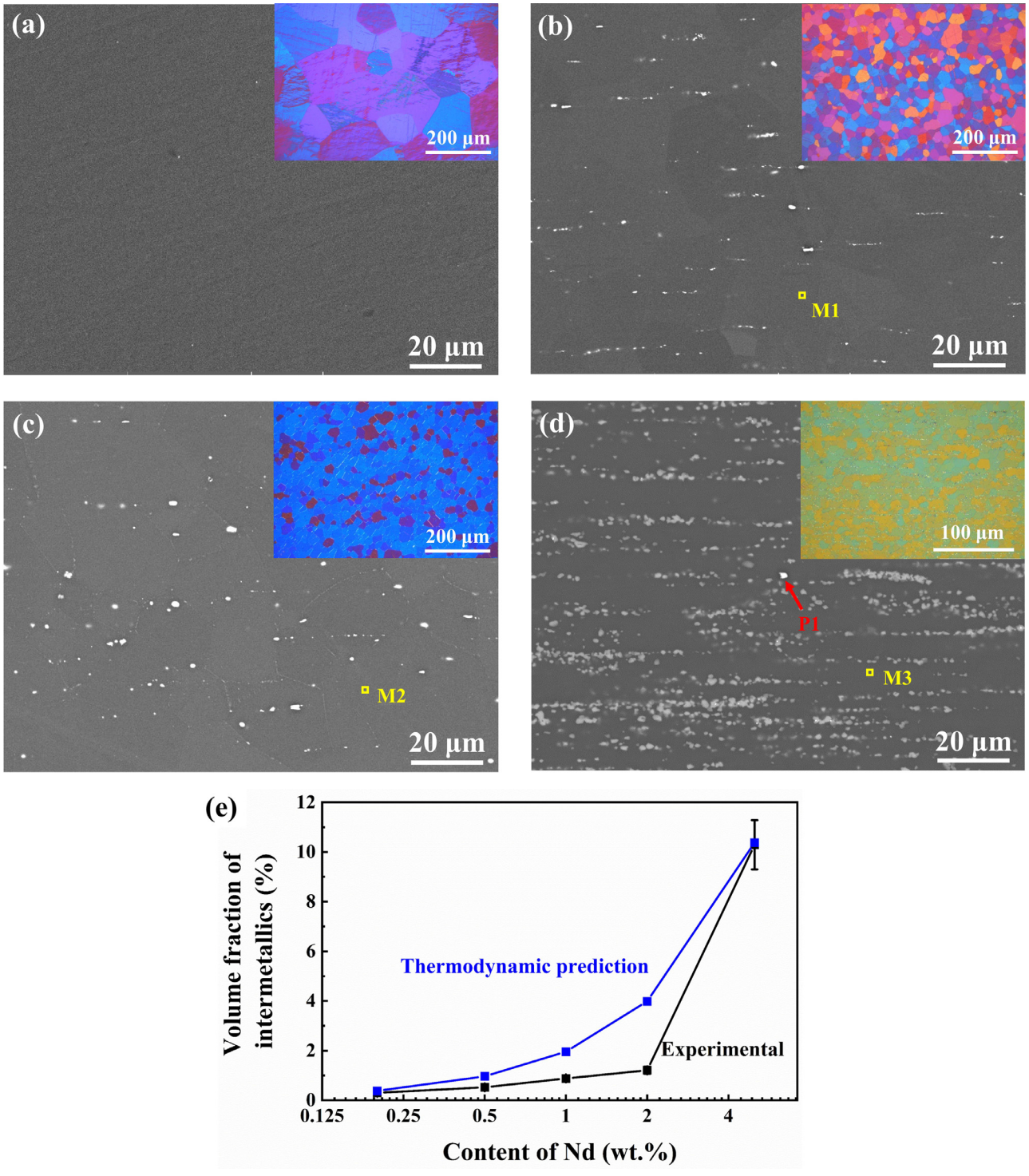

Fig. 4. BSE and optical micrographs of as-extruded pure Mg and Mg-Nd alloys along the extrusion direction: (a) pure Mg, (b) Mg-0.5Nd, (c) Mg-2Nd and (d) Mg-5Nd; together with (e) measured and simulated volume fraction of intermetallics in the as-extruded Mg-Nd alloys. The microstructure was observed on the longitudinal section.

Table 2
EDS results of as-extruded Mg-Nd alloy matrices and the impurity particle indicated in Fig. 4(d). "M" means the matrix and "P" the impurity particle.

Analysed locations	Alloys	Elements (wt. %)			
		Mg	Nd	Fe	Si
M1	Mg-0.5Nd	99.6 ± 0.1	0.4 ± 0.1	-	-
M2	Mg-2Nd	98.6 ± 0.1	1.4 ± 0.1	-	-
M3	Mg-5Nd	98.6 ± 0.1	1.4 ± 0.1	-	-
P1		48.8	25.3	16.5	9.4

Table 3
Grain sizes of as-extruded pure Mg and Mg-Nd alloys along the extrusion direction.

Alloys	Pure Mg	Mg-0.5Nd	Mg-2Nd	Mg-5Nd
Grain size (μm)	131.4 ± 76.0	24.7 ± 9.8	19.8 ± 8.0	9.5 ± 3.6

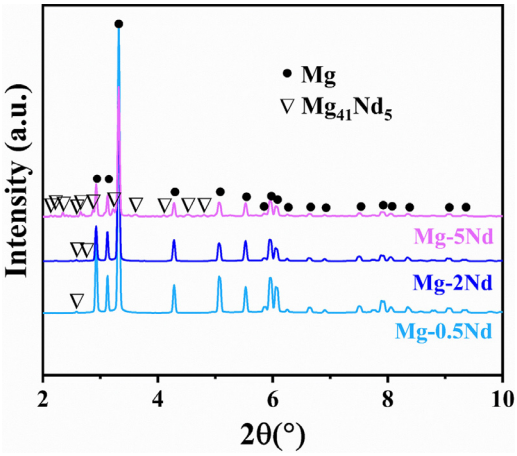

Fig. 5. Synchrotron radiation diffraction patterns of as-extruded Mg-Nd alloys.

1.4 ± 0.1 wt. %, demonstrating that the solid solution of Nd in Mg matrix was saturated. According to the binary Mg-Nd phase diagram, the maximum solubility of Nd in Mg is 3.6 wt. % at the Mg-Nd eutectic temperature [35]. At the present extrusion temperature 450°C, the solubility of Nd is approximately 1.2 wt. % in Mg. This value is close to the measured Nd content in the matrix of Mg-2Nd and Mg-5Nd alloys. In both the Mg-2Nd and Mg-5Nd alloys, the additional amount of Nd is more than its solubility limit. The part of Nd not going into solid solution in Mg matrix then exists in the form of second phases. These second phase particles are distributed along the extrusion direction. Most of them locate at grain boundaries (Fig. 4). With increasing the addition amount of Nd, both the experimental measurements and thermodynamic predictions show that their volume fraction increases (Fig. 4(f)). Experiment measurements demonstrated that the volume fraction of second phase increases from 0.5 ± 0.1% in the as-extruded Mg-0.5Nd to 10.3 ± 1.0% in the as-extruded Mg-5Nd. Fig. 4(f) further indicates the difference in the volume fraction of intermetallic compound exists between the experimental measurements and thermodynamic predictions. The volume fraction of intermetallic compound measured by the former is less than that predicted by the latter. Besides these intermetallic particles, a bright particle (indicated by the red arrow in Fig. 4(d)) containing impurity Fe and Si was detected in Mg-5Nd alloy (Table 2). It is likely a (Fe,Nd,Si)-containing compound. After adding the alloying element Nd into Mg, the average grain size of as-extruded Mg-Nd alloys significantly reduces (Table 3). It decreases with increasing the content of Nd. When the content of Nd increases to 5 wt. %, the as-extruded Mg-5Nd has the smallest grains.

Fig. 5 displays the synchrotron radiation diffraction patterns of as-extruded Mg-Nd alloys. All the as-extruded Mg-Nd alloys are mainly composed of two different phases, i.e. α-Mg and β-$Mg_{41}Nd_5$. This result is in agreement with that shown by the binary Mg-Nd phase diagram [35]. $Mg_{41}Nd_5$ is a eutectic phase which is an equilibrium phase in the binary Mg-Nd system. Among all the alloys, Mg-5Nd alloy has the highest intensity of β-$Mg_{41}Nd_5$ peaks, indicating this alloy has the maximum volume fraction of intermetallic compound. TEM observations (Fig. 6) showed that these globular $Mg_{41}Nd_5$ particles have a size of about 1 μm. As observed by SEM, they were mostly distributed at grain boundaries. A few of them can also be found inside grains. Further identification of selected area diffraction pattern confirms that they are $Mg_{41}Nd_5$ phase with a space group of I4/m and lattice parameters of a = 1.4743, b = 1.4743 and c = 1.0393 nm. This result is consistent with that identified using radiation diffraction patterns.

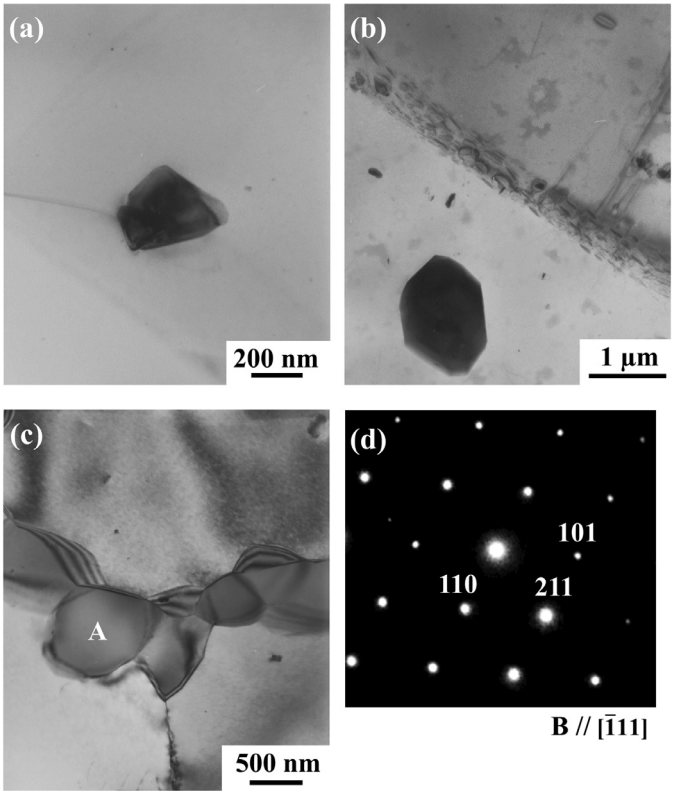

Fig. 6. TEM micrographs of as-extruded (a) Mg-0.5Nd, (b) Mg-2Nd, (c) Mg-5Nd and (d) the selected area electron diffraction of second phase A in Figure 6(c). The beam direction and zone axis are [$\bar{1}$11].

3.3. Degradation properties

3.3.1. Localized potential distribution

In the present investigation, Mg-5Nd alloy was selected for SKPFM characterizations since it has the highest amount of intermetallic compound and which makes it is easier to find $Mg_{41}Nd_5$ particles. Fig. 7 presents the topography map and its corresponding map of Volta potential distribution. Although the micro-constituents of the alloy are vague in the AFM topography image (Fig. 7(a)), they can still be differentiated distinctly based on their contrast difference (see the yellow arrows). Under the mode of

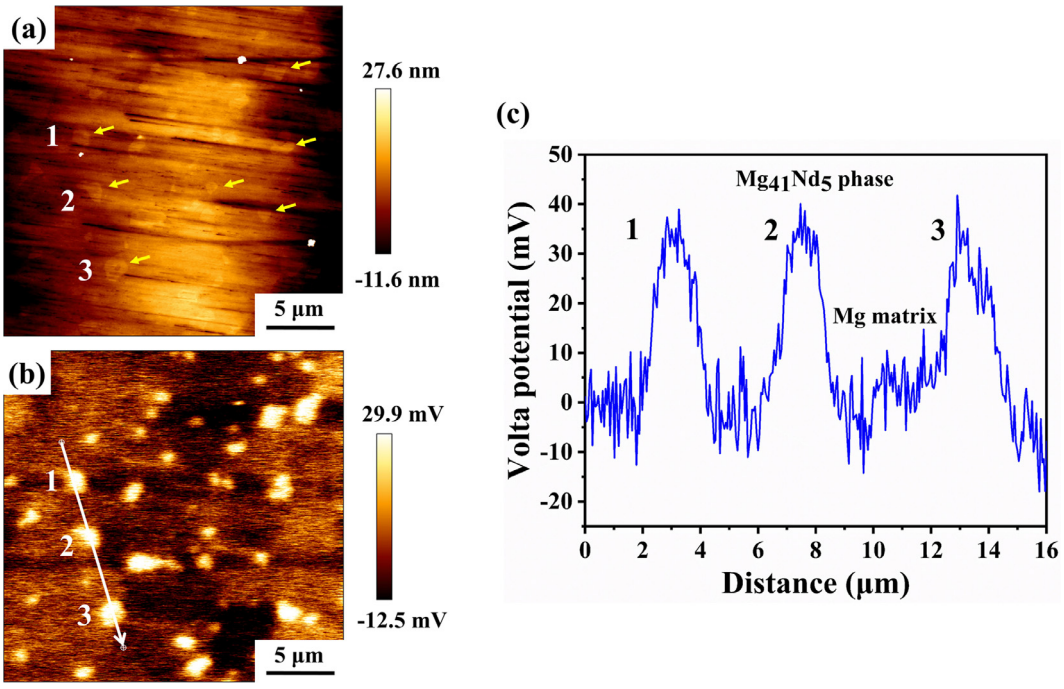

Fig. 7. SKPFM results of as-extruded Mg-5Nd alloy: (a) topography map, (b) surface Volta potential map, and (c) line-profile analysis of relative Volta potential through intermetallic $Mg_{41}Nd_5$ phase and Mg matrix.

Volta potential distribution, such contrast difference becomes very apparent between the intermetallic particles $Mg_{41}Nd_5$ and Mg matrix (Fig. 7(b)). The intermetallic particles exhibit much brighter contrast. In order to further understand the difference in Volta potential between the $Mg_{41}Nd_5$ particles and Mg matrix, a line-profile analysis was performed, along which three intermetallic particles exist (indicated as 1, 2 and 3 in Fig. 7(b)). Its corresponding profile of Volta potential difference was shown in Fig. 7(c). It can be seen clearly that the magnesium matrix has a lower Volta potential. The Volta potentials of all three particles are close with a value of about 35 mV.

3.3.2. Degradation rate

The degradation rate and mean degradation depth measured by immersion tests are given in Fig. 8(a-b), respectively. When the immersion time is short (5 hours and 1 day), the degradation rate increases with increasing content of Nd (Fig. 8(a)), indicating that the corrosion accelerates with an increase in the volume fraction of intermetallic compound $Mg_{41}Nd_5$. The as-extruded Mg-5Nd alloy exhibited the greatest level of degradation. With the immersion proceeding to 7 and 14 days, this situation changed, i.e. the corrosion rate did not change with the volume fraction of intermetallics monotonously any more. The as-extruded Mg-5Nd alloy did not have the highest corrosion rate. Its degradation rate continuously reduced, which is nearly half of that for the as-extruded Mg-2Nd alloy. Even after immersion for 14 days, its degradation rate 0.15 ± 0.02 mm/y is still half of that for Mg-2Nd alloy, which is comparable for that of the as-extruded pure Mg (0.12 ± 0.01 mm/y). At the later stage of immersion (≥ 7 days), Mg-2Nd alloy has the maximum corrosion rate instead of Mg-5Nd alloy.

Besides the determination of degradation rate, the mean degradation depth of each alloy was also calculated (Fig. 8(b)). At the beginning of immersion (5 hours and 1 day), the depth of the degradation layer is not so different for each alloy, but at the later stage of immersion, its difference becomes increasingly apparent. Mg-2Nd alloy shows a much higher value of mean degradation depth. With increasing the immersion time, the mean degradation depth linearly increases. The univariate linear regression model was therefore used to fit the experimental data and the obtained coefficient of determination (R^2) shows the goodness of fit. The slope of fitted curve could be considered as the mean degradation rate (µm/day) during 14 days immersion. Compare these four alloys, the Mg-2Nd alloy has the highest mean degradation rate with a value of 0.93 µm/day. The corrosion rates of the other three alloys are close with a value of approximately 0.32 ~ 0.38 μm/day.

The increase of pH value was monitored during each change of fresh medium (Fig. 8(c)). At the beginning of degradation, it has a high value for all alloys. With the degradation proceeding, it tends to be stable. After short immersion for less than1 day, the increase of pH value increases with the addition of Nd (Fig. 8(c)). Mg-5Nd alloy exhibits an increase of pH with a value of about 0.6 after immersion for 1 day. While for Mg-0.5Nd alloy the increase of pH value is only 0.3. However, after a longer immersion with more than 7 days, the evolution of pH increase is changed. The as-extruded Mg-5Nd shows a slower increase in pH than other alloys with lower Nd contents. After immersion for 14 days, the pH increase of Mg-5Nd alloy has a minimum value. Besides the increase of pH value, the degradation of Mg-Nd alloys was accompanied with the release of metal cations such as Mg^{2+} and Nd^{3+}. The released Nd ion concentration in the medium for the as-extruded Mg-2Nd and Mg-5Nd at different immersion durations was shown in Fig. 8(d). These two alloys shows quite different evolutions of the released Nd concentration with the degradation proceeding. For the as-extruded Mg-2Nd alloy, the dissolution of Nd progresses with the immersion. The concentration of released Nd ion increases from 3.2 ± 0.1 ppb after immersion for 1 day to 3711.4 ± 15.3 ppb after immersion for 14 days. In contrast, it almost keeps unchanged with a value of ~ 1.0 ± 0.1 ppb during the whole immersion duration for Mg-5Nd alloy. It should be noticed that at the beginning of degradation with immersion for less than 5 days, the evolution of Nd ion concentration for both alloys is quite stable. With the immersion proceeding no apparent increase was observed (see the grey box shown in Fig. 8(d)).

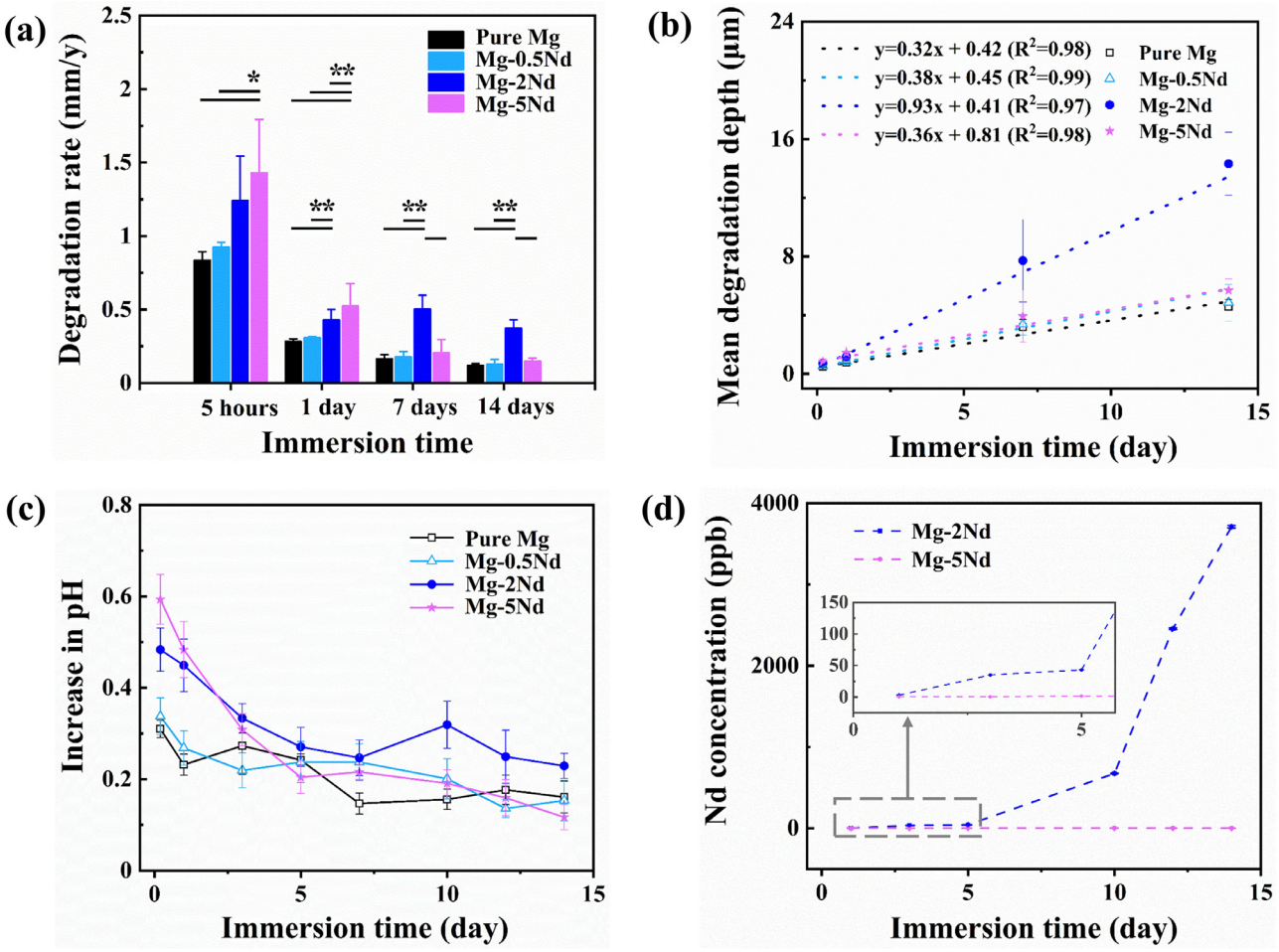

Fig. 8. (a) Degradation rate, (b) mean degradation depth, (c) increase in pH, (d) released Nd ion concentration in the medium. In Fig. 8(a), the statistical significance level is: * = p<0.05 and ** = p< 0.01. Fig. 8(b) displays both experimental values and fitted lines. In Fig. 8(d), the magnified grey solid box corresponds to the grey dot box.

Table 4
Element compositions at the selected points in Figure 9 by EDS analysis. "P" means the indicated particle.

Analysed locations	Elements (at. %)					
	O	Mg	C	P	Ca	Nd
P1	54.3	19.0	18.1	4.6	3.8	0.2
P2	18.4	71.0	4.5	0.8	0.5	4.8

3.3.3. Degradation morphology and composition

BSE micrographs of sample surfaces after degradation are depicted in Fig. 9. Cracks were observed on the surfaces of all samples due to the dehydrating when the samples were taken out of the immersion medium. Two corrosion product layers were observed on the surfaces of pure Mg, Mg-0.5Nd and Mg-2Nd alloys after their immersion for 1 day, i.e. inner layer and outer layer. On the top of inner layer in the Mg-2Nd alloy some small white products (indicated as P1 in Fig. 9) were found. These white products comprise high contents of Ca, P, C and O (Table 4), suggesting the formation of calcium-phosphate and carbonate particles. After long term immersion for 7 or 14 days such products grew and fully covered the inner layer. As for Mg-0.5Nd alloy, after immersion for 1 day the inner layer was nearly fully covered by the outer layer. Its surface was then completely covered by the corrosion layer during the subsequent immersion. The rough surface of sample after immersion for 7 days was caused by the processing procedure. In contrast, on the surface of Mg-5Nd alloy with high content of Nd only the outer layer was observed at different immersion time. The surface of the Mg-5Nd sample was covered by the growth of corrosion products after immersion for 7 or 14 days. The white particles (indicated as P2 in Fig. 9) were also observed on the corrosion layer after short immersion for 1 day. Unlike such white particles observed in Mg-2Nd alloy, they contain a higher content of Nd and Mg (Table 4), indicating that they were primarily $Mg_{41}Nd_5$ intermetallics rather than corrosion products. These intermetallic particles were exposed to the immersion medium as their surrounding matrix was corroded (Fig. 9). This result demonstrates that the intermetallic $Mg_{41}Nd_5$ cannot be degraded under the present corrosion condition.

The Nd content, Ca content and Ca/P ratio in the outer corrosion products on the surface of Mg-Nd alloys (0.5, 2 and 5 wt. % Nd) are shown (Fig. 10). First, at the beginning of corrosion, the outer layers of Mg-Nd alloys displayed a similar Ca/P atomic ratio with a value range of 0.5 ~ 0.7. The outer corrosion layer of Mg-5Nd alloy contained a higher content of Ca compared to other alloys with lower Nd contents. The Nd content in the outer corrosion layer increases with increasing the amount of Nd in Mg-Nd alloys. Among all alloys, the outer corrosion layer of Mg-5Nd alloy has the highest content of Nd, which is nearly twice of that for Mg-2Nd alloy. The obtained results illustrate that more Ca-Nd containing products should be formed in the outer surface corrosion layer of Mg-5Nd alloy at the initial stage of corrosion. Second, with the degradation proceeding, the content of Ca increases in the outer corrosion layer on the surfaces of Mg-Nd alloys. The evolution of

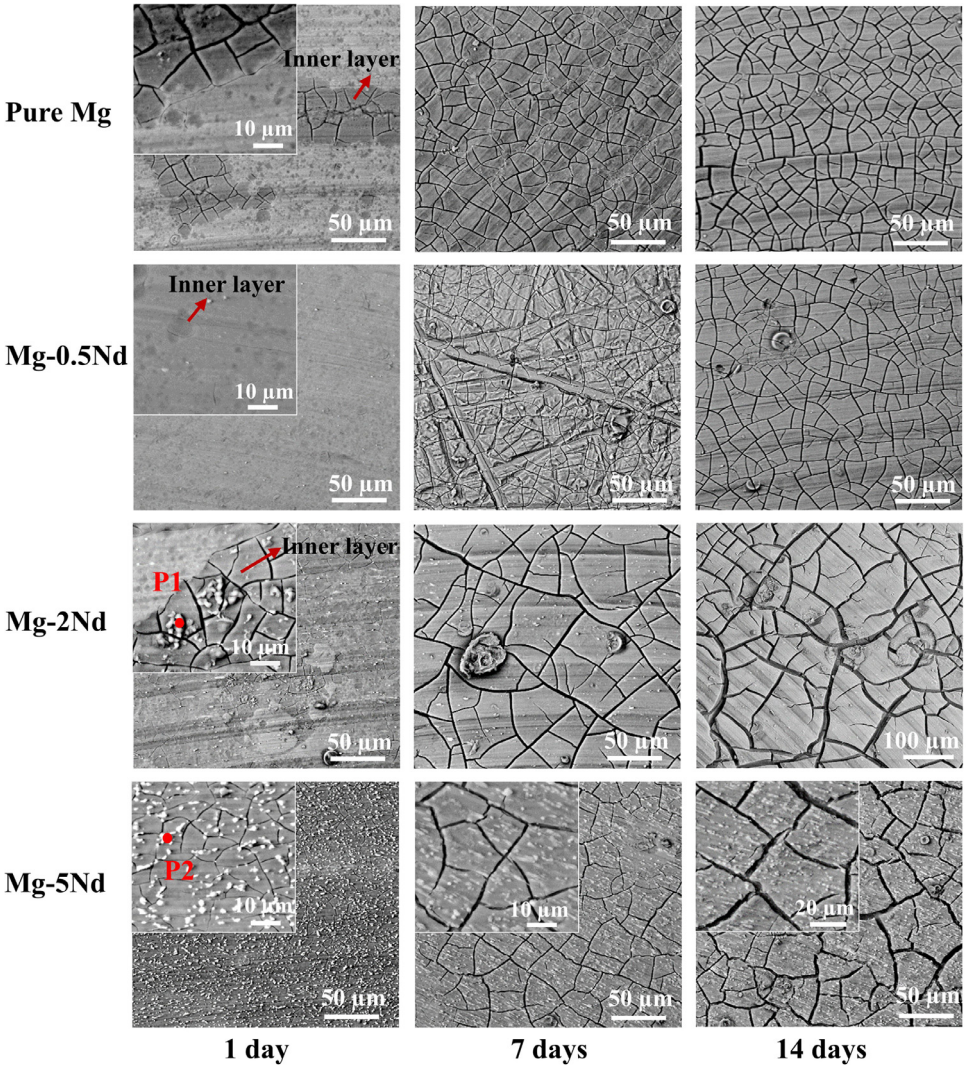

Fig. 9. BSE micrographs showing the surface morphologies of corrosion layers on the surfaces of as-extruded Mg-Nd alloys after different immersion durations.

Nd content in the outer corrosion layer of Mg-5Nd alloy is similar. But for those alloys with lower contents of Nd, the content of Nd in their outer surface corrosion layers has no apparent change. It keeps quite stable. Regarding the ratio of Ca/P in the outer surface corrosion layers, when immersed for 1 day or 7 days, it is very close for all alloys. However, after immersion for the longer time of 14 days, it increases almost double for Mg-5Nd alloy with a value of 1.3. Interestingly, the ratio of Ca/P in the outer surface corrosion layers still seems to remain unchanged for Mg-0.5Nd and Mg-2.0Nd alloys.

Fig. 11 shows the cross sectional BSE micrographs and corresponding elemental mappings for these samples after immersion for 14 days. It can be found that a compact corrosion layer was formed on the surfaces of bulk materials, which is strongly adhered to the matrix. Several interesting results can be summarized based on these morphologies of cross sectional corrosion layers and their elemental mappings. Firstly, with increasing the content of Nd to 2.0 wt. % the thickness of degradation layer increases, and then decreases with further increasing to 5.0 wt. % Nd (Fig. 11(d)). This result is consistent with that characterized by the degradation rate. Secondly, as shown by elemental mappings, the degradation products mainly contained Mg, Ca, P, C and O, indicating the formation of calcium-phosphate products and/or carbonate salts. Besides these elements, the alloying element Nd was also identified in the corrosion products. This is in agreement with that obtained by the EDS analysis of the corrosion surface (Table 4). Thirdly, the distributions of elements Ca, P and Nd in the corrosion layers are different for the different alloys. In the outer corrosion layer of all alloys the enrichment of Ca and P was observed. An Nd-rich corrosion layer was only detected in the as-extruded Mg-2Nd alloy, but in other alloys it could not be found (Fig. 11(b) and (d)). This Nd-rich corrosion layer is present near the interface between the matrix and inner degradation layer (as marked by the red arrow in Fig. 11(c)). Moreover, it should be noted that on the surface of as-extruded Mg-2Nd alloy the outer formed Ca-P rich layer was discontinuous. In contrast, a continuous Ca-P rich layer was observed on the surface of other alloys. Finally, as indicated by Fig. 11(b-d), the intermetallic particles $Mg_{41}Nd_5$ remained at their original sites. After corrosion they were integrated in the degradation product layer. When the Mg matrix was preferentially dissolved these "isolated" intermetallic particles were then embedded by the growth of corrosion products.

3.3.4. Characterizations of degradation products

Fig. 12 shows the synchrotron radiation diffraction spectra of corrosion products on the surfaces of as-extruded Mg-Nd alloys

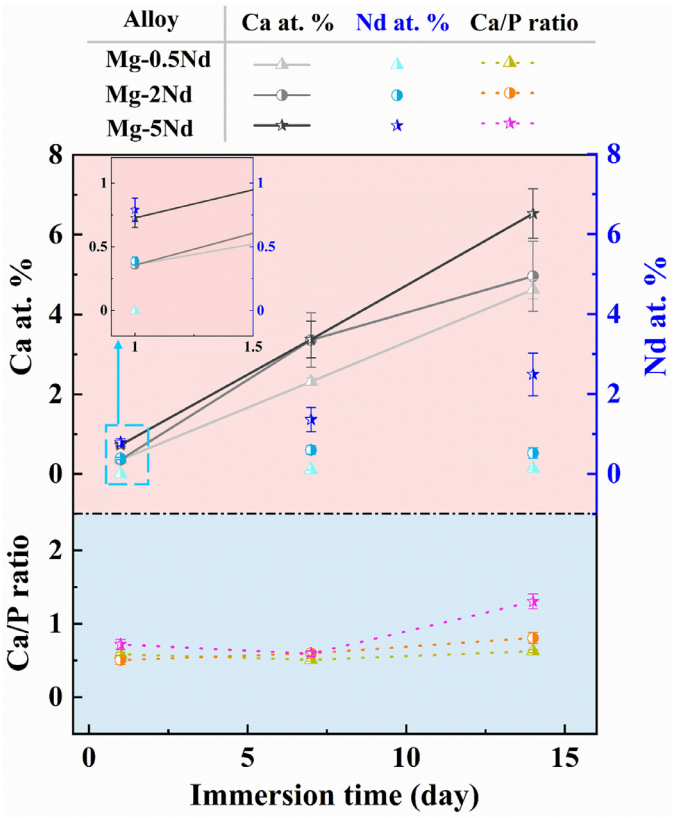

Fig. 10. Ca content, Nd content and Ca/P ratio in the corrosion products on the surface. The black "Line and Symbol" series correspond to the Ca content and blue "Scatter" series the Nd content. The magnified black solid box corresponds to the blue dot box.

after immersion for 1, 7 and 14 days. After short immersion for 1 and 7 days (indicated by green and blue dot lines with arrows in Fig. 12, respectively), fewer degradation products were formed on the surfaces of these samples. Their corrosion layers were very thin. The inner and outer layer could not be separated to be identified by the selected beam with a size of 5 μm × 10 μm. As for the same alloy, the same diffraction patterns were obtained for both the inner and outer corrosion layers. No different peaks could be identified. On such diffraction patterns, a broad diffraction peak with low intensity (marked by light blue background in Fig. 12), which is located at about 0.3~0.7°, was observed for all the corrosion layers. This indicates that the resultant corrosion products could be amorphous-like and/or contain nano-crystallites, as previously shown by Agha *et al.* [36] and Hou *et al.* [37]. With searching the crystallographic database of inorganic materials, this broad peak possibly corresponds to magnesium carbonate, magnesium phosphate or calcium phosphate. If only based on this broad diffraction peak it is difficult to distinguish and identify the degradation products accurately. After degradation for 14 days (labelled by the dotted red line in Fig. 12), with the thickness of corrosion layer increasing, more information could be obtained from the diffraction spectra. Firstly, the broad peak located at about 0.3~0.7° was still observed, indicating the main corrosion products for all alloys are the same, possibly being magnesium carbonate, magnesium phosphate or calcium phosphate. Even for pure magnesium, such a broad peak always exists, demonstrating that the alloying element Nd has no influence on its formation. Interestingly, although both the inner and outer corrosion layers still have similar diffraction patterns, indicating that their corrosion products should be the same, if the "broad" peak of inner corrosion layer is compared with that of outer layer located at 0.3~0.7°, the former has a small width. Such a phenomena indicates that crystallization could occur for the corrosion products from the outer to the inner of corrosion layer. Secondly, besides this aforementioned broad peak located at 0.3~0.7°, one additional small peak labelled with red heart appeared. It was identified as Dypingite ($Mg_5(CO_3)_4(OH)_2{\cdot}8H_2O$). It should be noticed that the diffraction pattern of this corrosion product also includes this broad peak located at 0.3~0.7°. Especially, the strongest peaks of Dypingite ($Mg_5(CO_3)_4(OH)_2{\cdot}8H_2O$) match with the broad peak. Finally, a comparison between the diffraction patterns of outer and inner corrosion layers for all four alloys after immersion for 14 days, showed that with an increase of Nd content the intensity of this additional small peak located at about 0.25° increases. However, the identifications of diffraction patterns indicated that no Nd, Ca and P containing corrosion products existed. This inconsistency with above mentioned EDS analysis results might be caused by their presence in the amorphous state or their amount less than the limit of synchrotron radiation detection.

In order to identify whether Nd-containing products were formed in the corrosion layer, the as-extruded Mg-2Nd and Mg-5Nd samples after immersion for 14 days were selected for ToF-SIMS analysis (Fig. 3). Fig. 13 shows their BSE micrographs, Nd-relevant positive mass spectra and secondary ion maps in their local areas (indicated by blue dot rectangle). Owing to the limitation of the ToF-SIMS instrument, the elements with their mass up to 172 (m/Q) can only be detected. In the mass spectra of both the as-extruded Mg-2Nd and Mg-5Nd samples, peaks associated with Ga ions (primary ion source) and Nd-containing ions (Nd^+, NdH^+, NdO^+, $NdOH^+$) were observed. Among these ions, the secondary ions of $^{142}Nd^+$, $^{142}Nd^{16}O^+$, $^{146}Nd^1H^+$ and $^{146}Nd^{16}O^1H^+$, which have a higher intensity than other isotopes, were selected for further mapping. Their map results showed that for the as-extruded Mg-2Nd sample $^{142}Nd^+$, $^{142}Nd^{16}O^+$ and $^{146}Nd^{16}O^1H^+$ ions were enriched in the area close to the interface between the matrix and corrosion (indicated by red arrows in Fig. 13). As for $^{146}Nd^1H^+$ ion with its lower intensity, its distributions is quite homogeneous. No regions enriched with this ion was characterized. The similar map results were obtained for the as-extruded Mg-5Nd sample. Like in Mg-2Nd alloy, both the $^{146}Nd^+$ and $^{146}Nd^{16}O^+$ signals were also stronger in the area close to the matrix (indicated by red arrows, Fig. 13(b)). In contrast, the signals of $^{146}Nd^1H^+$ and $^{146}Nd^{16}O^1H^+$ ions were very weak making it difficult to observe their distributions in the surface corrosion layer. Considering the type of detected Nd ions, the Nd-containing corrosion products in the inner layer (close to the matrix) should be neodymium oxide and/or neodymium hydroxide.

4. Discussion

4.1. Microstructure

According to the Mg-Nd phase diagram [35], Nd has a low solid solubility with a value of 3.67 wt. % at the eutectic temperature and nearly zero at room temperature in Mg matrix. If the content of added Nd is over this limit it precipitates out to form $Mg_{41}Nd_5$ or $Mg_{12}Nd$. In the present as-extruded Mg-Nd alloys, only the $Mg_{41}Nd_5$ phase was identified. Our previous investigation indicated that $Mg_{12}Nd$ phase was formed during solidification [38]. It transformed to $Mg_{41}Nd_5$ phase during hot extrusion. This result was further confirmed by the identifications of present synchrotron radiation diffraction and TEM observations (Figs. 5 and 6).

During solidification, the solute Nd atoms segregated at the solid / liquid interface, resulting in constitutional supercooling in the diffusion layer ahead of the advancing solid / liquid interface.

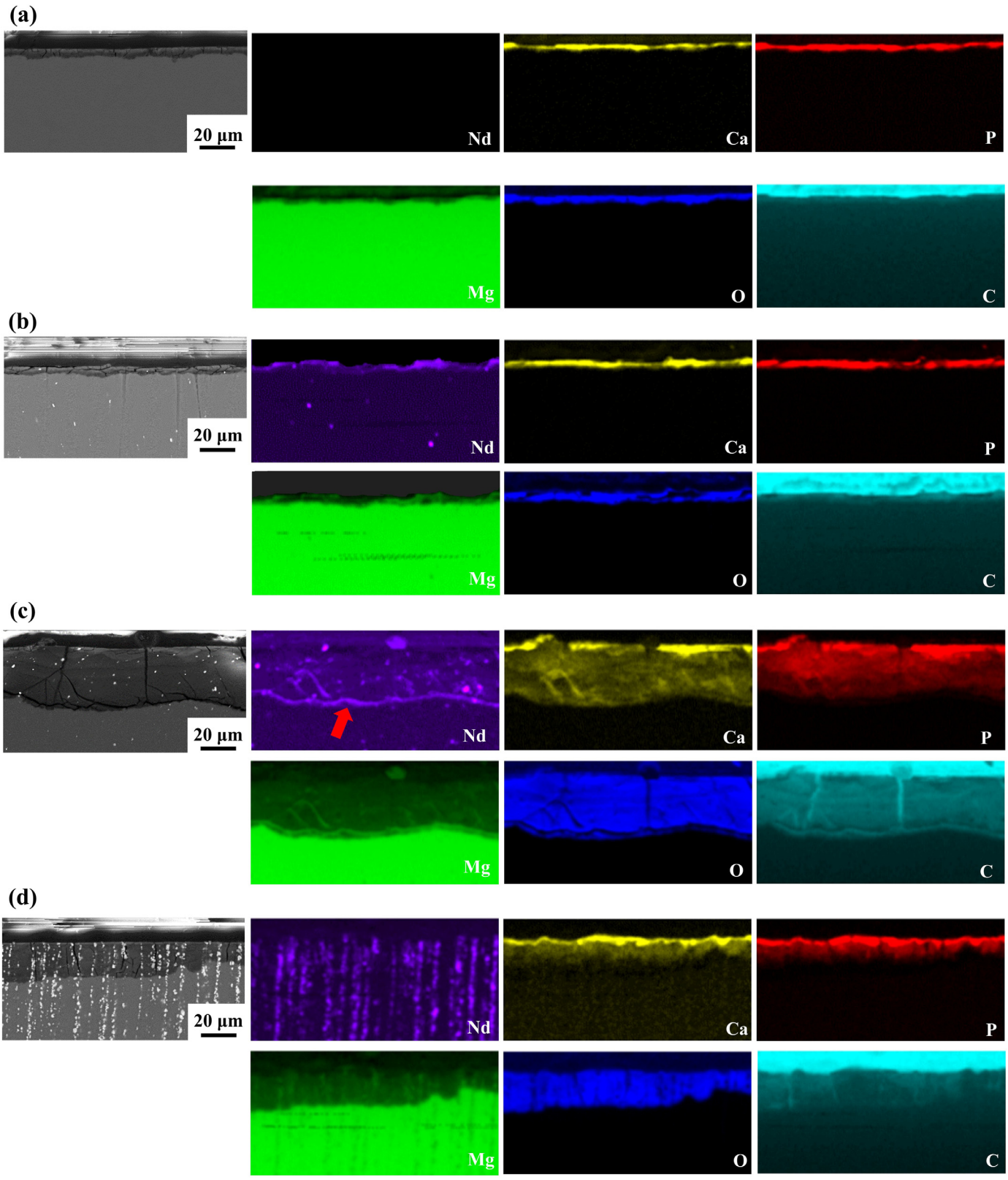

Fig. 11. Cross-sectional BSE micrographs and corresponding element mappings of as-extruded (a) pure Mg, (b) Mg-0.5Nd, (c) Mg-2Nd and (d) Mg-5Nd alloys exposed to DMEM + 10% FBS under cell culture conditions for 14 days. Red arrow marks Nd-rich corrosion product.

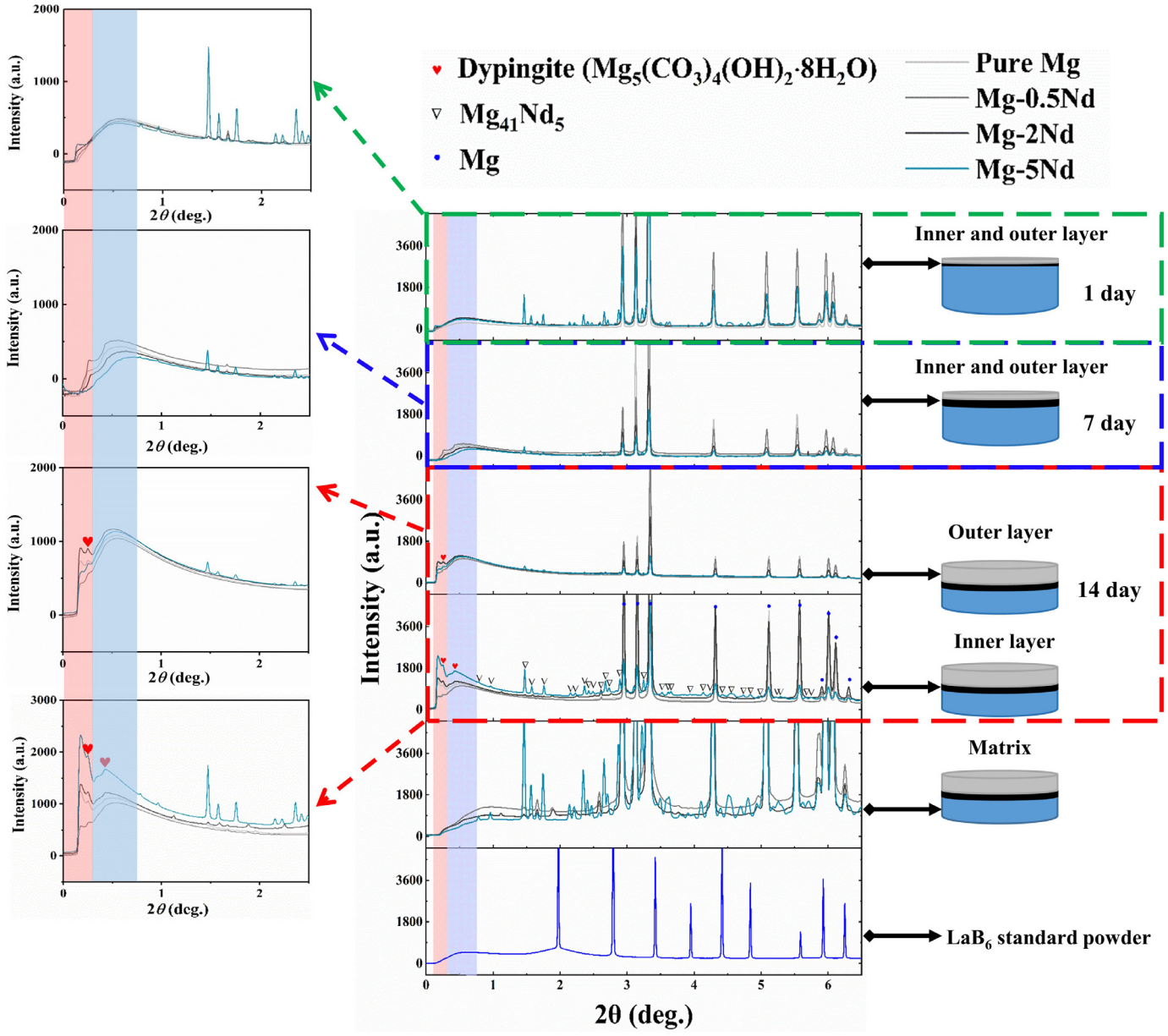

Fig. 12. Synchrotron radiation diffraction patterns of degradation products by line scan analysis after 1, 7 and 14 days of immersion. The images and arrows on the right mark the positions where detected.

This constitutional supercooling is a major driving force for the nucleation of α-Mg [39]. Owing to the present high cooling rate associated with direct chill casting, the diffusion of solute Nd in the melt was possibly retarded. The proceeding of present solidification was considered to be under a non-equilibrium condition. Thus, the non-equilibrium Scheil solidification model was used to calculate the volume fraction of intermetallic phase in Mg-Nd alloys. Comparing the experimental and theoretical data in Fig. 4, it can be found that the amount of intermetallics measured based on the BSE micrographs is relatively lower than the calculated value. This can be explained by the following two aspects. Firstly, it can be attributed to the statistical error due to the non-uniform distribution of second phase, especially in the Mg-Nd alloys with low contents of Nd (Fig. 4). Secondly, a homogenization annealing treatment at 440°C was performed before the hot extrusion. During this treatment a part of second phase was dissolved. In the subsequent hot extrusion at 450°C, this part of Nd could not be precipitated out yet.

After hot extrusion, the grains were greatly refined. The extrusion temperature was 450°C. Under such a high temperature and at an extrusion ratio of 1: 63, the dynamic recrystallization (DRX) should occur. In fact, Fig. 4 verifies that equiaxed grains were obtained for all alloys due to the occurrence of dynamic recrystallization. In addition, with increasing the content of Nd the grain size reduces. This should be caused by the increased amount of $Mg_{41}Nd_5$ particles in Mg-Nd alloys. During hot extrusion, the existence of undissolved $Mg_{41}Nd_5$ particles could enhance the nucleation of dynamic recrystallization. A strain gradient occurred between the thermally stable $Mg_{41}Nd_5$ particles and surrounding matrix, which created a region with high dislocation density and large orientation gradient. DRX nucleation was therefore accelerated based on a typical particle stimulating nucleation (PSN) mechanism [40,41]. Moreover, the existence of these $Mg_{41}Nd_5$ particles could act as obstacles to the grain boundary migration and retarded the grain growth.

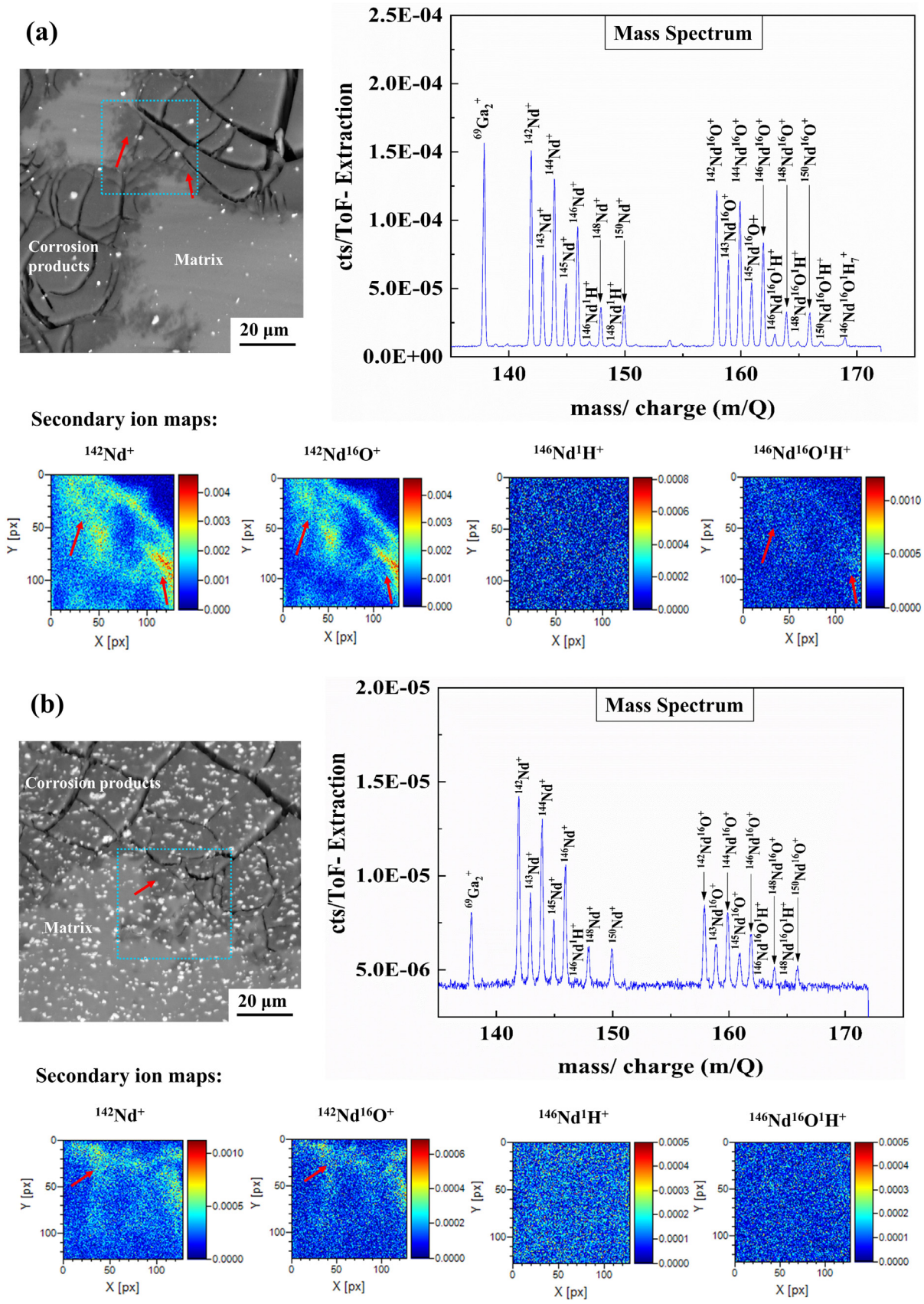

Fig. 13. BSE micrographs, Nd-relevant positive mass spectra and secondary ion maps of local areas between the matrix and inner corrosion layer in the extruded (a) Mg-2Nd and (b) Mg-5Nd alloys after immersion for 14 days. Red arrows indicate the areas with ion signals.

4.2. Degradation properties

4.2.1. Factors influencing the corrosion of Mg-Nd alloys

In this section, the possible factors to affect the corrosion of Mg-Nd alloys are discussed. The aim is to clarify that the intermetallic microstructure including its amount and distribution plays a dominant role in influencing the corrosion of Mg-Nd alloys. In contrast, the effects of other factors on corrosion of Mg-Nd alloys could be neglected or they do not disturb or confuse the obtained results and final conclusions.

Regarding the present as-extruded Mg-Nd series, the factors to affect their corrosion include the following factors, the impurities such as iron, second phase, solubility of solute Nd in Mg, grain size and texture. The degradation rate of Mg-Nd alloys can be described as:

$$DR = DR_{Mg} + \Delta DR_{Pre} + \Delta DR_{CP} + \Delta DR_{GS} + \Delta DR_{SS} + \Delta DR_{Tex} + \Delta DR_{IMP} \quad (2)$$

where DR is the degradation rate of Mg-Nd alloys in a corrosive medium, DR_{Mg} is the intrinsic reactivity of Mg, ΔDR_{Pre} is the effect of precipitates or second phases on the corrosion rate, ΔDR_{CP} is the influence of corrosion products, ΔDR_{GS} is the influence of grain size on the corrosion rate, ΔDR_{SS} is the influence of alloying elements with solid solution in Mg matrix, ΔDR_{Tex} is the effect from texture, and ΔDR_{IMP} is the effect from impurities such as iron.

Our previous investigations demonstrated that the textures in Mg-Nd alloys were quite weak because of the existence of alloying element Nd [42]. Their influence on the corrosion could be neglected [38]. As shown by Table 1, in both the present Mg-0.5Nd and Mg-5Nd alloys, the contents of impurity Fe are relatively high. Before discussing the effects of intermetallic amount on the corrosion of Mg-Nd alloys, it is necessary to clarify whether its existence disturbs the obtained results and final conclusions. After deliberating about the following points, its disturbance is also considered to be disregarded. Firstly, as mentioned in the previous work [21,38,43], iron could react with Nd to form (Fe, Nd)-containing intermetallics, which was supported by EDS analysis (Table 2 and Fig. 4). Its harmful influence on the corrosion was then weakened. Secondly, previous results that the existence of iron in magnesium deteriorates its corrosion resistance sharply were obtained based on the investigations in such corrosion media NaCl solutions. Our preliminary results indicate that when iron containing magnesium alloys was immersed in DMEM + 10% FBS, its harmful effect on the corrosion resistance was not so apparent as that observed in NaCl solution [44]. The detailed results will be published later. Thirdly, the corrosion of alloys did not follow the previous conclusion: the higher content of impurity Fe their higher corrosion rate. For example, comparing the as-extruded Mg-0.5Nd and Mg-2Nd alloys, the former with a lower amount of intermetallics has a higher content of Fe (Table 1), but shows a lower degradation rate than Mg-2Nd alloy with more intermetallics (Fig. 8(a)). This demonstrates that, the corrosion was mainly influenced by micro-galvanic corrosion between $Mg_{41}Nd_5$ particles and Mg matrix rather than by that between impurity particles and Mg matrix. Moreover, at the later stage of corrosion (Fig. 8), although Mg-5Nd alloy has the highest content of iron its corrosion rate is much lower than that of Mg-2Nd alloy. This result further elucidates that iron did not play a main role in affecting the corrosion of present Mg-Nd alloys.

It is well known that grain size influences the corrosion resistance [45,46]. Previous investigations concluded that a fine microstructure is beneficial for improving the corrosion resistance of magnesium alloys [47,48]. After hot extrusion the grains of Mg-Nd alloys were refined. The grain size reduces with an increase of Nd content, i.e. decreases with increasing the amount of intermetallics. Unlike the previous results, the present corrosion results did not show that the corrosion resistance of Mg-Nd alloys improves with reducing the grain size not only at the earlier stage of corrosion but also at the later stage of corrosion. At the earlier stage of corrosion, the degradation rate (Fig. 8(a)) increases with increasing the content of Nd even though the grain size reduces. While at the later stage of corrosion, i.e. after immersion for 7 days or 14 days, the as-extruded Mg-2Nd alloy having the fine grains shows the highest degradation rate (Fig. 8(a)). It could be concluded that ΔDR_{GS} has a very small effect on corrosion behaviour of binary Mg-Nd alloys compared to the factor of intermetallic factor ΔDR_{Pre}.

The solid solution of solutes in the Mg matrix could change its chemical potential, and consequently they affect the corrosion resistance of magnesium alloys. In the present investigation, EDS analysis indicated that the solubility limit of Nd in Mg matrix is about 1.4 wt. % (Table 2). When the addition of Nd is more than 2 wt. %, the content of Nd in Mg matrix remains unchanged. In the as-extruded Mg-0.5Nd alloy, almost all Nd atoms went into solution in Mg matrix. Based on the previous results [24,38,49], the solid solution of Nd in Mg matrix could improve its corrosion resistance. The improvement of corrosion resistance is proportional to the solid solubility of Nd. In this way, with increasing the content of Nd from 0 to 2 wt. % in Mg-Nd alloys, their corrosion resistance should be improved. Moreover, if the aforementioned point's influence caused by grain size is considered, their improvement of corrosion resistance should be significantly more apparent [47,48]. Actually, that is not the truth. At the earlier stage of corrosion, with increasing the content of Nd the corrosion resistance conversely decreases (Fig. 8(a)). This further elucidates that the solid solubility of Nd and grain size are not the dominant factors to influence the corrosion of Mg-Nd alloys.

In summary, the intermetallic microstructure including its amount and distribution plays a key role in affecting the corrosion of present Mg-Nd alloys. The Eq. (2) is then simplified:

$$DR = DR_{Mg} + \Delta DR_{Pre} + \Delta DR_{CP} \quad (3)$$

In the following sections, the discussion about the influence of intermetallic microstructure on corrosion is focused, including its amount and distribution. In fact, the intermetallic distribution is closely related with its amount. Thus, they were discussed together.

4.2.2. Effects of intermetallic amount and its distribution on the corrosion

4.2.2.1. Role of intermetallic microstructure at the earlier stage of corrosion (immersion for 5 hours or 1 day). Microstructural observations indicated that only one second phase $Mg_{41}Nd_5$ existed in the as-extruded Mg-Nd alloys (Figs. 5 and 6). Compared with the Mg matrix, this phase has a higher localized potential (Fig. 7). It can serve as a local cathode. When immersed in DMEM + 10% FBS, the micro-galvanic corrosion could initiate in Mg matrix around these "isolated" $Mg_{41}Nd_5$ particles [50]:

$$Mg + 2\,H_2O \rightarrow Mg^{2+} + 2\,(OH^-) + H_2 \quad (4)$$

The degradation of magnesium matrix promoted the pH value of corrosion media (Fig. 8(c)). This was also confirmed by our previous investigation [38]. When such galvanic corrosion started, the Mg matrix also started its degradation accompanied by the formation corrosion products and the corrosion layer. Apparently, such galvanic corrosion is proportional to the amount of $Mg_{41}Nd_5$ particles. That is to say, it increases with increasing the amount of intermetallics. Owing to the fact that the formation of the corrosion layer was incomplete and discontinuous on the surface of Mg-Nd alloys (Fig. 9), its influence on the corrosion proceeding was not so apparent. It can be believed that at the earlier stage of corrosion, the degradation of Mg matrix proceeded by such galvanic

corrosion should be dominant. Correspondingly, the intermetallic amount plays an important role in influencing the corrosion initiation and proceeding. That is why when immersed for 5 hours or 1 day with increasing the content of Nd the corrosion resistance was deteriorated.

4.2.2.2. Role of intermetallic microstructure in affecting the formation of corrosion layer. As the corrosion proceeds, the corrosion products and corrosion layer are formed on the surface of Mg-Nd alloys. Especially for such alloys with higher content of Nd, their formations should be much quicker. Once the complete and continuous corrosion layer was formed on the surface, its effects on the subsequent corrosion should not be neglected. It could affect the diffusion of ions coming from the degraded Mg matrix and corrosion media, and consequently influence the corrosion proceeding. Based on the present results, it can be concluded that both the continuity and compactness of the corrosion layer are closely related with the amount of intermetallic particles $Mg_{41}Nd_5$ in Mg-Nd alloys.

The amount of intermetallic particles $Mg_{41}Nd_5$ affects the micro-galvanic corrosion and the speed to form a connected corrosion layer on the surface of as-extruded Mg-Nd alloys. After immersion for 1 day, a complete corrosion layer was observed on the surface of Mg-5Nd alloy, but not on the surfaces of other alloys (Fig. 9). In this alloy with 5 wt. % Nd the amount of intermetallic particles $Mg_{41}Nd_5$ is maximum. The separation distance between each particle is the shortest. As a result, the corrosion proceeding around such densely distributed particles made it quick to connect corrosion products with each other and to form the continuous corrosion layer, which were mainly the carbonates (discussed in detail later). Accompanying the quick corrosion at the beginning, the release of Nd^{3+} was also higher for Mg-5Nd alloy than that for other alloys (Fig. 10). ToF-SIMS results verified that in the corrosion layer Nd was detected, demonstrating that during immersion the alloying element Nd interacted with corrosion media to form Nd-containing corrosion products. They are possibly neodymium oxide and/or neodymium hydroxide, i.e. Nd_2O_3 and $Nd(OH)_3$ [51–53] formed by the following reactions:

$$2\ Nd\ +\ 3\ H_2O\ \rightarrow\ Nd_2O_3{+}3\ H_2 \tag{5}$$

$$2\,Nd + 6H_2O \rightarrow 2\,Nd(OH)_3 + 3\,H_2 \tag{6}$$

Nd_2O_3 is insoluble in water. $Nd(OH)_3$ is slightly soluble with a solubility of approximately 1.3×10^{-33}, which is much smaller than that of $Mg(OH)_2$ (5.6×10^{-12}) [54,55]. Owing to their insolubility, Nd_2O_3 and $Nd(OH)_3$ remained in the corrosion layer during corrosion. It was reported that the presence of neodymium oxide in the corrosion layer could enhance the corrosion resistance [51,56]. Such a Nd-containing corrosion layer greatly inhibited the penetration of the detrimental Cl^- [24,57]. In addition, Nd_2O_3 has a Pilling-Bedworth ratio with more than 1. Its presence is beneficial for improving the compactness of the corrosion layer and for protecting the alloy matrix from further corrosion [58]. Thus, regarding the role of intermetallic particles $Mg_{41}Nd_5$ in affecting the corrosion, very interestingly two conflicting roles can be summarized, which was termed as “coin effect”. One is their negative role, i.e. their existence enhances the micro-galvanic corrosion. Another is their positive role, their existence, especially for the existence of the high amount of intermetallic particle, favours the formation of continuous and compact corrosion layer.

The amount of intermetallic particles $Mg_{41}Nd_5$ influences whether a compact corrosion layer could be formed on the surfaces of Mg-Nd alloys. When the content of Nd is less than 2 wt. %, at the earlier stage of immersion the less galvanic corrosion around the sparsely distributed $Mg_{41}Nd_5$ particles could not produce enough corrosion products to cover the alloy surface completely (Fig. 9). Under such a situation, the incomplete surface corrosion layer could not block the inward and outward diffusion of ions effectively. The Nd^{3+} released by the degradation of matrix could easily diffuse into the corrosion solution. Indeed, the measurement of Nd^{3+} concentration in the corrosion solution of Mg-2Nd alloy indicated that it continuously increased with the corrosion proceeding (Fig. 8(d)). While the content of Nd is lower in the surface corrosion layer and kept unchanged in the whole immersion (Fig. 10). Both of these two phenomena elucidates that less Nd^{3+} could be frozen and less Nd-containing corrosion products could be formed in the corrosion layer on the surface of Mg-2Nd alloy. Even at the later stage of immersion, the formed corrosion layer was not compact. It could not block the diffusion of Nd^{3+} effectively. In contrast, when the content of Nd reaches to 5 wt. %, a complete corrosion layer could quickly be formed after immersion only for 1 day (Fig. 9). In this alloy, the distribution of intermetallic particles is quite dense. The large amount of galvanic corrosion around $Mg_{41}Nd_5$ particles allowed the corrosion products to connect with each other easily and quickly. In addition, the present results prove that the corrosion layer on the surface of Mg-5Nd alloy was also compact. Unlike in Mg-2Nd alloy, it could effectively block the release of Nd^{3+} into the corrosion solution. This is supported by EDS analysis of the surface corrosion layer with high content of Nd detected (Fig. 10) and the measurement of the Nd^{3+} concentration in the corrosion medium that was remained unchanged during the entire immersion (Fig. 8(d)).

The compactness of the corrosion layer formed on the surface of Mg-Nd alloys subsequently influenced the outward diffusion of Nd^{3+} and Mg^{2+} and inward diffusion of corrosive agent ions. Such an influence resulted in the formation of Ca-P layer on the surface of the corrosion layer and the occurrence of a Nd-rich layer at the interface between the corrosion layer and Mg matrix (Fig. 11). The present investigation results indicated that the Nd-containing corrosion layer is quite compact. It could effectively hinder the diffusions of ions such as Nd^{3+}, Ca^{2+}, PO_4^{3-} and HPO_4^{2-} etc. [24,57]. As for the Mg-5Nd alloy, due to the fact that a complete and compact corrosion layer was formed on its surface early, the ions Ca^{2+}, PO_4^{3-} and HPO_4^{2-} etc. could not diffuse inwards easily. They deposited on the surface of the corrosion layer to form a continuous Ca-P layer (Fig. 11). In fact, the present EDS analysis of surface corrosion layer demonstrated that with the corrosion proceeding the ratio of Ca/P increased (Fig. 10). It is reasonable to expect that it was significantly more difficult for the Ca^{2+} with a larger atomic radius to diffuse through the corrosion layer. As a result, more Ca was detected on the surface of corrosion layer. In contrast, as for the other alloys, owing to the fact that a compact corrosion layer could not be formed on their surface, the formed Ca-P layer on its top was discontinuous. That the Ca-P rich layer was formed on the top of corrosion layer is in agreement with that obtained by many previous *in vitro* [34,37,59] and *in vivo* degradation [60–62] investigations. According to the compositions of DMEM [32], it is known that Ca^{2+}, PO_4^{3-} and HPO_4^{2-} ions exist. When magnesium alloys were exposed to the DMEM, the following reaction occurred [37,63,64]:

$$x\,Mg^{2+} + y\,Ca^{2+} + z\,PO_4^{3-} \rightarrow Mg_xCa_y(PO_4)_z \tag{7}$$

The corrosion product $Mg_xCa_y(PO_4)_z$ was then formed in the corrosion layer. Moreover, for Mg-2Nd alloy after immersion for 14 days an Nd-rich layer near the interface between the corrosion layer and Mg matrix was observed (Fig. 11(c)). For this alloy, it was easier for the agent ions to diffuse through its corrosion layer because of its looseness. The inward corrosion therefore proceeded quickly at the interface. In such a region more Mg-Nd solid solution was degraded. Consequently, more Mg^{2+} and Nd^{3+} were then released. Owing to the much faster diffusion of Mg^{2+} in the corrosion layer, it made Nd^{3+} remain at the interface.

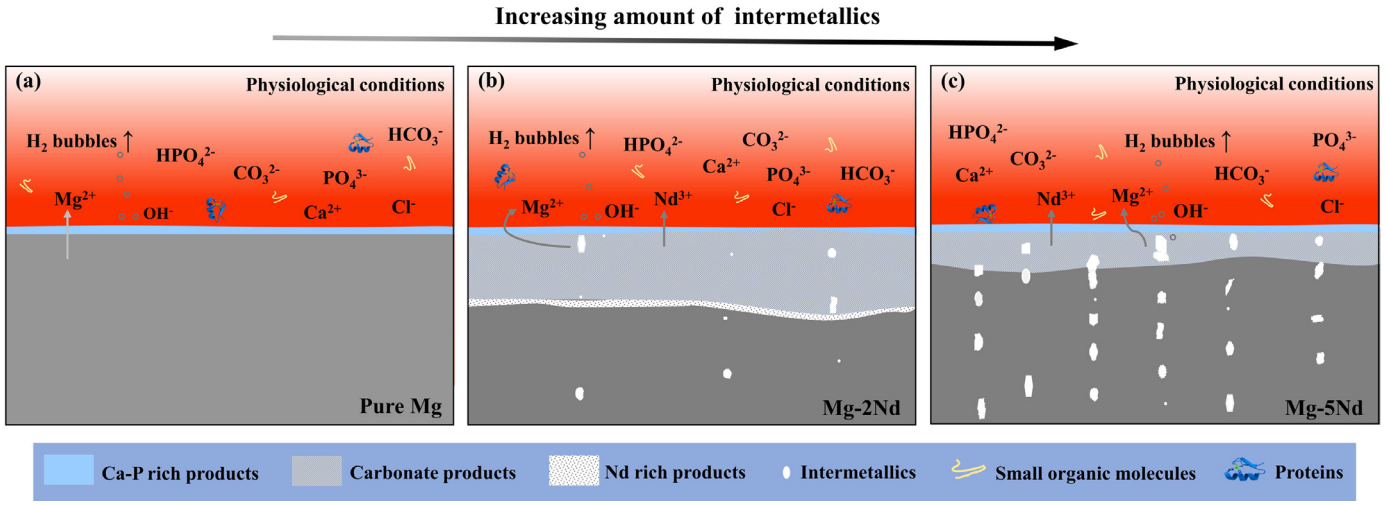

Fig. 14. Schematic illustration of the degradation of as-extruded Mg-Nd alloys with different amount of intermetallic phases at the later stage of immersion.

In summary, a schematic model is suggested to depict the degradation of as-extruded Mg-Nd alloys under physiological conditions (Fig. 14). Fig. 14(a) depicts the dissolution of pure Mg and Mg^{2+} going into the solution. Fig. 14(b) and (c) indicate that $Mg_{41}Nd_5$ particles in Mg-Nd alloys remain undegradable under physiological conditions. With the existence of these cathodic $Mg_{41}Nd_5$ particles, magnesium dissolution was promoted due to the micro-galvanic corrosion. The corrosion of Mg-Nd alloys is controlled by the aforementioned "coin" effect of $Mg_{41}Nd_5$ intermetallic amount, i.e. high cathodic activity of these intermetallic particles (micro-galvanic corrosion) and their favour for the formation of protective surface layers. Fig. 14(b) shows that the protective effect of corrosion products cannot counteract the deterioration caused by galvanic corrosion. Corrosion propagates towards the matrix with the enrichment of Nd at the interface between the matrix and corrosion layer. In Fig. 14(c), the protection from the compact corrosion layers is balanced with the deterioration caused by the intermetallic particles $Mg_{41}Nd_5$, resulting in the uniform distribution of Nd in the corrosion layers.

4.2.3. Influence of intermetallic amount on the microstructure of corrosion products

Microstructural characterizations indicated that the present corrosion products are mainly the carbonate and calcium-phosphate products. At the earlier stage of immersion, it is difficult to identify their crystal structures (Fig. 12). They are amorphous existing in the corrosion layer, as proven by previous work [36,37]. In the present work, after immersion for the long duration of 14 days, the crystallization of carbonate products was also detected in the inner layer. These carbonate products were then identified as dypingite ($Mg_5(CO_3)_4(OH)_2{\cdot}8H_2O$). In fact, many previous in vitro tests have indicated the carbonate products formed under physiological conditions were primarily nesquehonite ($MgCO_3{\cdot}3H_2O$) and/or $Mg_5(CO_3)_4(OH)_2{\cdot}\ xH_2O$ [37,65,66]. It was reported that nesquehonite can transform to dypingite after heating at 35°C for 224 hours. It transforms faster at a higher temperature [67]. It is reasonable to deduce that nesquehonite was formed at the early stage of immersion (1 and 7 days). With increasing the immersion time to 14 days at 37°C, it finally transformed to dypingite. Besides these carbonate products, EDS analysis and ToF-SIMS results show that other corrosion products also existed, including calcium-phosphate, neodymium oxide and/or hydroxide. However, they could not be identified by synchrotron radiation owing to their peak's broadening. They should exist in the corrosion layer in amorphous or nano-crystallized state.

Present microstructural characterisations demonstrated that the intermetallic particles $Mg_{41}Nd_5$ remained in the corrosion layer. They were undegradable. Their existence in the corrosion layer seems to enhance the crystallization of corrosion products (Fig. 12). With increasing the content of Nd, the amount of intermetallic particles $Mg_{41}Nd_5$ increases. As a result, the amount of sites supplied for inhomogeneous nucleation of corrosion products also increased. This is beneficial for the crystallization of corrosion products with immersion proceeding. Correspondingly, the peak located at 0.3~0.7° (marked by the second red heart) becomes increasingly narrower.

4.2.4. Influence of Nd content (intermetallic amount) on corrosion resistance

Based on the aforementioned discussion, the amount of intermetallic particles $Mg_{41}Nd_5$ plays an important role in affecting the initiation of micro-galvanic corrosion, the formation of a compact corrosion layer, the outward diffusion of ions released by the matrix degradation and the inward diffusion of corrosion agent ions. After understanding such effect mechanisms, it is not dificult to explain how the content of Nd or the amount of intermetallic compounds in Mg-Nd alloys affects their corrosion resistance. The influence of Nd on the corrosion resistance of Mg-Nd alloys mainly depends on which "coin effect" of intermetallic particles, the negative role or positive role, is dominant. At the early stage of immersion, the negative role of intermetallic particles $Mg_{41}Nd_5$, i.e. the micro-galvanic corrosion, predominated. Thus, with increasing the content of Nd, the amount of intermetallic particles $Mg_{41}Nd_5$ increases, the corrosion resistance of Mg-Nd alloys was then deteriorated (Fig. 8).

At the later stage of immersion, when the corrosion product was connected with each other and a continuous layer covered the surface of Mg-Nd alloys, besides the negative role of these intermetallic particles, their positive role in influencing the corrosion resistance must also be considered. When this positive role was dominant, the compact corrosion layer mainly influences the subsequent corrosion proceeding. Mg-5Nd alloy has the greatest amount of intermetallic particles. Among all alloys, the formation of continuous and compact corrosion layer is the earliest. Its Ca-P layer on the top of the corrosion layer is continuous. Consequently, at the later stage of immersion, this Mg-5Nd alloy shows the best corrosion resistance. Under such a "coin effect" of intermetallic particles $Mg_{41}Nd_5$, i.e. the interaction of their positive and negative roles in affecting the corrosion resistance, at the later stage of corrosion, the corrosion rate of Mg-Nd alloys first increases with

increasing the content of Nd, then reaches a maximum, and with a further increase of Nd content, it begins to decreases (Fig. 8).

5. Conclusion

The influence of intermetallic amount on the corrosion resistance was investigated by immersing Mg-Nd alloys with different contents of Nd into DMEM+ 10% FBS. The following conclusions were reached:

- In the as-extruded Mg-Nd alloys, $Mg_{41}Nd_5$ particles are distributed throughout their matrix with a size of about 1 μm. Their amount increases with increasing the content of Nd.
- The existence of intermetallic particles $Mg_{41}Nd_5$ affects the corrosion of Mg-Nd alloys in two conflicting ways. One is their negative role that their existence enhances the micro-galvanic corrosion. Another is their positive role that their existence favours the formation of a continuous and compact corrosion layer.
- At the early stage of immersion, the negative role of intermetallic particles $Mg_{41}Nd_5$ in influencing the corrosion is dominant. The corrosion resistance of Mg-Nd alloys is deteriorated by increasing the content of Nd or the amount of intermetallic particles $Mg_{41}Nd_5$.
- At the later stage of corrosion, owing to the interaction between the positive and negative roles of intermetallic particles $Mg_{41}Nd_5$ in affecting the corrosion resistance, the corrosion rate of Mg-Nd alloys first increases with increasing the content of Nd, then reaches the maximum at 2 wt. % Nd. With a further increase of the content of Nd it begins to decreases.
- The main corrosion products include carbonates, calcium-phosphate, neodymium oxide and/or neodymium hydroxide. They are amorphous at the early stage of immersion. With the immersion proceeding, they are transformed to crystalline. The existence of undegradable $Mg_{41}Nd_5$ particles in the corrosion layer can enhance the crystallization of amorphous corrosion products.

Declaration of Competing Interest

The authors declare that they have no known competing financial interests or personal relationships that could have appeared to influence the work reported in this paper.

Acknowledgments

We acknowledge DESY (Hamburg, Germany), a member of the Helmholtz Association HGF, for the provision of experimental facilities. Parts of this research were carried out at PETRA III and we would like to thank Dr. Norbert Schell for assistance in using the HEMS beamline. Mr. Gert Wiese in MagIC is also gratefully acknowledged for the technical support. The author Yaping Zhang would like to thank the China Scholarship Council for the award of a fellowship and funding (No. 201604910708).

References

[1] F. Witte, N. Hort, C. Vogt, S. Cohen, K.U. Kainer, R. Willumeit-Römer, F. Feyerabend, Degradable biomaterials based on magnesium corrosion, Curr. Opin. Solid State Mater. Sci. 12 (5) (2008) 63–72.
[2] F. Witte, Reprint of: The history of biodegradable magnesium implants: a review, Acta Biomater. 23 (2015) 28–40.
[3] M.P. Staiger, A.M. Pietak, J. Huadmai, G. Dias, Magnesium and its alloys as orthopedic biomaterials: a review, Biomaterials 27 (9) (2006) 1728–1734.
[4] N. Ikeo, M. Nishioka, T. Mukai, Fabrication of biodegradable materials with high strength by grain refinement of Mg-0.3 at.% Ca alloys, Mater. Lett. 223 (2018) 65–68.
[5] S. Sandlobes, Z. Pei, M. Friak, L.F. Zhu, F. Wang, S. Zaefferer, D. Raabe, J. Neugebauer, Ductility improvement of Mg alloys by solid solution: ab initio modeling, synthesis and mechanical properties, Acta Mater. 70 (2014) 92–104.
[6] P. Hidalgo-Manrique, J.D. Robson, M.T. Perez-Prado, Precipitation strengthening and reversed yield stress asymmetry in Mg alloys containing rare-earth elements: a quantitative study, Acta Mater. 124 (2017) 456–467.
[7] J.F. Nie, Precipitation and hardening in magnesium alloys, Metal. Mater. Trans. A 43 (11) (2012) 3891–3939.
[8] M.C. Zhao, M. Liu, G.L. Song, A. Atrens, Influence of the β-phase morphology on the corrosion of the Mg alloy AZ91, Corros. Sci. 50 (7) (2008) 1939–1953.
[9] X.B. Liu, D.Y. Shan, Y.W. Song, E.H. Han, Influence of yttrium element on the corrosion behaviors of Mg-Y binary magnesium alloy, J. Magnesium Alloys 5 (1) (2017) 26–34.
[10] J.H. Liu, Y.W. Song, J.C. Chen, P. Chen, D.Y. Shan, E.H. Han, The special role of anodic second phases in the micro-galvanic corrosion of EW75 Mg alloy, Electrochim. Acta 189 (2016) 190–195.
[11] L. Yang, Y.D. Huang, F. Feyerabend, R. Willumeit-Römer, K.U. Kainer, N. Hort, Influence of ageing treatment on microstructure, mechanical and bio-corrosion properties of Mg-Dy alloys, J. Mech. Behav. Biomed. Mater. 13 (2012) 36–44.
[12] W.R. Zhou, Y.F. Zheng, M.A. Leeflang, J. Zhou, Mechanical property, biocorrosion and in vitro biocompatibility evaluations of Mg-Li-(Al)-(RE) alloys for future cardiovascular stent application, Acta Biomater. 9 (10) (2013) 8488–8498.
[13] L.L. Shi, Y.D. Huang, L. Yang, F. Feyerabend, C. Mendis, R. Willumeit-Römer, K.U. Kainer, N. Hort, Mechanical properties and corrosion behavior of Mg-Gd-Ca-Zr alloys for medical applications, J. Mech. Behav. Biomed. Mater. 47 (2015) 38–48.
[14] A. Srinivasan, Y.D. Huang, C.L. Mendis, C. Blawert, K.U. Kainer, N. Hort, Investigations on microstructures, mechanical and corrosion properties of Mg-Gd-Zn alloys, Mater. Sci. Eng. 595 (2014) 224–234.
[15] G. Song, A.L. Bowles, D.H. StJohn, Corrosion resistance of aged die cast magnesium alloy AZ91D, Mater. Sci. Eng. 366 (1) (2004) 74–86.
[16] D. Song, A.B. Ma, J.H. Jiang, P.H. Lin, D.H. Yang, J.F. Fan, Corrosion behaviour of bulk ultra-fine grained AZ91D magnesium alloy fabricated by equal-channel angular pressing, Corros. Sci. 53 (1) (2011) 362–373.
[17] Y.W. Song, E.H. Han, D.Y. Shan, C.D. Yim, B.S. You, The effect of Zn concentration on the corrosion behavior of Mg-xZn alloys, Corros. Sci. 65 (2012) 322–330.
[18] J. Kubásek, D. Vojtěch, Structural characteristics and corrosion behavior of biodegradable Mg-Zn, Mg-Zn-Gd alloys, J. Mater. Sci. Mater. Med. 24 (7) (2013) 1615–1626.
[19] S. Cai, T. Lei, N. Li, F. Feng, Effects of Zn on microstructure, mechanical properties and corrosion behavior of Mg-Zn alloys, Mater. Sci. Eng. 32 (8) (2012) 2570–2577.
[20] Y.S. Jeong, W.J. Kim, Enhancement of mechanical properties and corrosion resistance of Mg-Ca alloys through microstructural refinement by indirect extrusion, Corros. Sci. 82 (2014) 392–403.
[21] N. Birbilis, M.A. Easton, A.D. Sudholz, S.M. Zhu, M.A. Gibson, On the corrosion of binary magnesium-rare earth alloys, Corros. Sci. 51 (3) (2009) 683–689.
[22] J. Meng, W. Sun, Z. Tian, X. Qiu, D. Zhang, 2-Corrosion performance of magnesium (Mg) alloys containing rare-earth (RE) elements, in: G.L. Song (Ed.), Corrosion Prevention of Magnesium Alloys, Ed., Woodhead Publishing, 2013, pp. 38–60.
[23] A.D. Sudholz, K. Gusieva, X.B. Chen, B.C. Muddle, M.A. Gibson, N. Birbilis, Electrochemical behaviour and corrosion of Mg-Y alloys, Corros. Sci. 53 (6) (2011) 2277–2282.
[24] J. KubÁSek, D. VojtĚCh, Structural and corrosion characterization of biodegradable Mg-RE (RE=Gd, Y, Nd) alloys, Trans. Nonferrous Metals Soc. China 23 (5) (2013) 1215–1225.
[25] M. Liu, P. Schmutz, P.J. Uggowitzer, G. Song, A. Atrens, The influence of yttrium (Y) on the corrosion of Mg-Y binary alloys, Corros. Sci. 52 (11) (2010) 3687–3701.
[26] F.R. Elsayed, N. Hort, M.A. Salgado Ordorica, K.U. Kainer, Magnesium permanent mold castings optimization, Mater. Sci. Forum (2011) 65–68.
[27] V. Kree, J. Bohlen, D. Letzig, K. Kainer, The metallographical examination of magnesium alloys, Praktische Metallographie-Practical Metallography 41 (5) (2004) 233–246.
[28] N. Hort, V. Floss, S. Gavras, G. Wiese, D. Tolnai, Metallography of Mg, in: V.V. J. e. al. (Ed.) The Mineral, Metals & Materials Society 2019, San Antonio, Texas, 2019.
[29] ASTM E112-13Standard Test Methods for Determining Average Grain Size, ASTM International, 2013.
[30] C. Zhang, J. Miao, S. Chen, F. Zhang, A.A. Luo, CALPHAD-based modeling and experimental validation of microstructural evolution and microsegregation in magnesium alloys during solidification, J. Phase Equilibria Diffus. 40 (4) (2019) 495–507.
[31] E.P.S. Nidadavolu, F. Feyerabend, T. Ebel, R. Willumeit-Römer, M. Dahms, On the determination of magnesium degradation rates under physiological conditions, Materials (Basel) 9 (8) (2016) 627.
[32] J. Fischer, M.H. Prosenc, M. Wolff, N. Hort, R. Willumeit-Römer, F. Feyerabend, Interference of magnesium corrosion with tetrazolium-based cytotoxicity assays, Acta Biomater. 6 (5) (2010) 1813–1823.
[33] E. ISO, 10993-122008-Biological evaluation of medical devices-Part 12: Sample preparation and reference materials (ISO 10993-12: 2007), German version: DIN EN ISO, 2008 10993-10912.
[34] R. Hou, J. Victoria-Hernandez, P. Jiang, R. Willumeit-Römer, B. Luthringer-Feyerabend, S. Yi, D. Letzig, F. Feyerabend, In vitro evaluation of the ZX11 magnesium alloy as potential bone plate: degradability and mechanical integrity, Acta Biomater. 97 (2019) 608–622.

[35] S. Gorsse, C.R. Hutchinson, B. Chevalier, J.F. Nie, A thermodynamic assessment of the Mg-Nd binary system using random solution and associate models for the liquid phase, J. Alloys Compd. 392 (1) (2005) 253–262.
[36] N.A. Agha, Z.D. Liu, F. Feyerabend, R. Willumeit-Römer, B. Gasharova, S. Heidrich, B. Mihailova, The effect of osteoblasts on the surface oxidation processes of biodegradable Mg and Mg-Ag alloys studied by synchrotron IR microspectroscopy, Mater. Sci. Eng. 91 (2018) 659–668.
[37] R.Q. Hou, N. Scharnagl, F. Feyerabend, R. Willumeit-Römer, Exploring the effects of organic molecules on the degradation of magnesium under cell culture conditions, Corros. Sci. 132 (2018) 35–45.
[38] Y. Zhang, Y. Huang, F. Feyerabend, S. Gavras, Y. Xu, R. Willumeit-Römer, K.U. Kainer, N. Hort, Effects of intermetallic microstructure on degradation of Mg-5Nd alloy, Metal. Mater. Trans. A 51 (2020) 5498–5515.
[39] Y. Lee, A. Dahle, D. StJohn, The role of solute in grain refinement of magnesium, Metal. Mater. Trans. A 31 (11) (2000) 2895–2906.
[40] F.J. Humphreys, The nucleation of recrystallization at second phase particles in deformed aluminium, Acta Metall. 25 (11) (1977) 1323–1344.
[41] Y.L. Liu, D. Juul Jensen, N. Hansen, Recovery and recrystallization in Cold-Rolled Al-SiCw composites, Metall. Trans. A 23 (3) (1992) 807–819.
[42] K. Hantzsche, J. Bohlen, J. Wendt, K.U. Kainer, S.B. Yi, D. Letzig, Effect of rare earth additions on microstructure and texture development of magnesium alloy sheets, Scr. Mater. 63 (7) (2010) 725–730.
[43] S. Han, S. Mu, J. Du, Effects of Ce and Y on modification and corrosion behavior of Mg-0.8% Si alloy: A correlation study, Corrosion 75 (9) (2019) 1100–1109.
[44] Y. Zhang, Y. Huang, B. Luthringer-Feyerabend, R. Willumeit-Römer, K.U. Kainer, N. Hort, Unpublished results.
[45] K. Ralston, N. Birbilis, Effect of grain size on corrosion: a review, Corrosion 66 (7) (2010) 075005-075005-13.
[46] G. Song, D. StJohn, The effect of zirconium grain refinement on the corrosion behaviour of magnesium-rare earth alloy MEZ, J. Light Met. 2 (1) (2002) 1–16.
[47] G. Argade, S. Panigrahi, R. Mishra, Effects of grain size on the corrosion resistance of wrought magnesium alloys containing neodymium, Corros. Sci. 58 (2012) 145–151.
[48] Q. Liu, Q.X. Ma, G.Q. Chen, X. Cao, S. Zhang, J.L. Pan, G. Zhang, Q.Y. Shi, Enhanced corrosion resistance of AZ91 magnesium alloy through refinement and homogenization of surface microstructure by friction stir processing, Corros. Sci. 138 (2018) 284–296.
[49] L. Yang, L. Ma, Y. Huang, F. Feyerabend, C. Blawert, D. Höche, R. Willumeit-Römer, E. Zhang, K.U. Kainer, N. Hort, Influence of Dy in solid solution on the degradation behavior of binary Mg-Dy alloys in cell culture medium, Mater. Sci. Eng. 75 (2017) 1351–1358.
[50] A. Atrens, G.L. Song, Z.M. Shi, A. Soltan, S. Johnston, M.S. Dargusch, Understanding the corrosion of Mg and Mg alloys, reference module in chemistry, Mol. Sci. Chem. Eng. (2018) 515–534.
[51] Y. Song, Y.H. Liu, S. Yu, X. Zhu, S. Wang, Effect of neodymium on microstructure and corrosion resistance of AZ91 magnesium alloy, J. Mater. Sci. 42 (12) (2007) 4435–4440.
[52] H. Ardelean, A. Seyeux, S. Zanna, F. Prima, I. Frateur, P. Marcus, Corrosion processes of Mg-Y-Nd-Zr alloys in Na_2SO_4 electrolyte, Corros. Sci. 73 (2013) 196–207.
[53] J. Ninlachart, K.S. Raja, Threshold chloride concentration for passivity breakdown of Mg-Zn-Gd-Nd-Zr alloy (EV31A) in basic solution, Acta Metallurgica Sinica (English Letters) 30 (4) (2017) 352–366.
[54] J.A. Dean, Lange's handbook of chemistry, McGraw-Hill, Inc., New york; London, 1999.
[55] M. Pourbaix, J. Burbank, Atlas D-equilibres electrochimiques, The Electrochemical Society, 1964.
[56] G. Levy, E. Aghion, Effect of diffusion coating of Nd on the corrosion resistance of biodegradable Mg implants in simulated physiological electrolyte, Acta Biomater. 9 (10) (2013) 8624–8630.
[57] H.B. Yao, Y. Li, A.T.S. Wee, J.S. Pan, J.W. Chai, Correlation between the corrosion behavior and corrosion films formed on the surfaces of $Mg_{82-x}Ni_{18}Nd_x$ (x=0, 5, 15) amorphous alloys, Appl. Surf. Sci. 173 (1) (2001) 54–61.
[58] S.D. Cramer, B.S. Covino, ASM Handbook, Corrosion: Fundamentals, Testing, and Protection, 13, A, ASM international, 2003.
[59] Y. Zong, G. Yuan, X. Zhang, L. Mao, J. Niu, W. Ding, Comparison of biodegradable behaviors of AZ31 and Mg-Nd-Zn-Zr alloys in Hank's physiological solution, Mater. Sci. Eng. 177 (5) (2012) 395–401.
[60] L. Xu, G. Yu, E. Zhang, F. Pan, K. Yang, In vivo corrosion behavior of Mg-Mn-Zn alloy for bone implant application, Journal of Biomedical Materials Research Part A 83 (3) (2007) 703–711.
[61] Z. Li, X. Gu, S. Lou, Y. Zheng, The development of binary Mg-Ca alloys for use as biodegradable materials within bone, Biomaterials 29 (10) (2008) 1329–1344.
[62] P.K. Bowen, J. Drelich, J. Goldman, Magnesium in the murine artery: Probing the products of corrosion, Acta Biomater. 10 (3) (2014) 1475–1483.
[63] L. Yang, E. Zhang, Biocorrosion behavior of magnesium alloy in different simulated fluids for biomedical application, Mater. Sci. Eng. 29 (5) (2009) 1691–1696.
[64] M. Kieke, F. Feyerabend, J. Lemaitre, P. Behrens, R. Willumeit-Römer, Degradation rates and products of pure magnesium exposed to different aqueous media under physiological conditions, BioNanoMaterials 17 (3-4) (2016) 131–143.
[65] D. Mei, S.V. Lamaka, J. Gonzalez, F. Feyerabend, R. Willumeit-Römer, M.L. Zheludkevich, The role of individual components of simulated body fluid on the corrosion behavior of commercially pure Mg, Corros. Sci. 147 (2019) 81–93.
[66] R. Willumeit-Römer, J. Fischer, F. Feyerabend, N. Hort, U. Bismayer, S. Heidrich, B. Mihailova, Chemical surface alteration of biodegradable magnesium exposed to corrosion media, Acta Biomater. 7 (6) (2011) 2704–2715.
[67] A.L. Harrison, V. Mavromatis, E.H. Oelkers, P. Bénézeth, Solubility of the hydrated Mg-carbonates nesquehonite and dypingite from 5 to 35°C: implications for CO_2 storage and the relative stability of Mg-carbonates, Chem. Geol. 504 (2019) 123–135.